AD-A040 823 SOUTHWEST RESEARCH INST SAN ANTONIO TEX F/G 11/4
INVESTIGATION OF FIRST PLY FAILURE IN GRAPHITE/EPOXY LAMINATES --ETC(U)
JUN 76 P H FRANCIS, D E WALRATH, D N WEED F33615-75-C-5115
UNCLASSIFIED AFML-TR-77-62 NL

1 OF 1
AD A040823

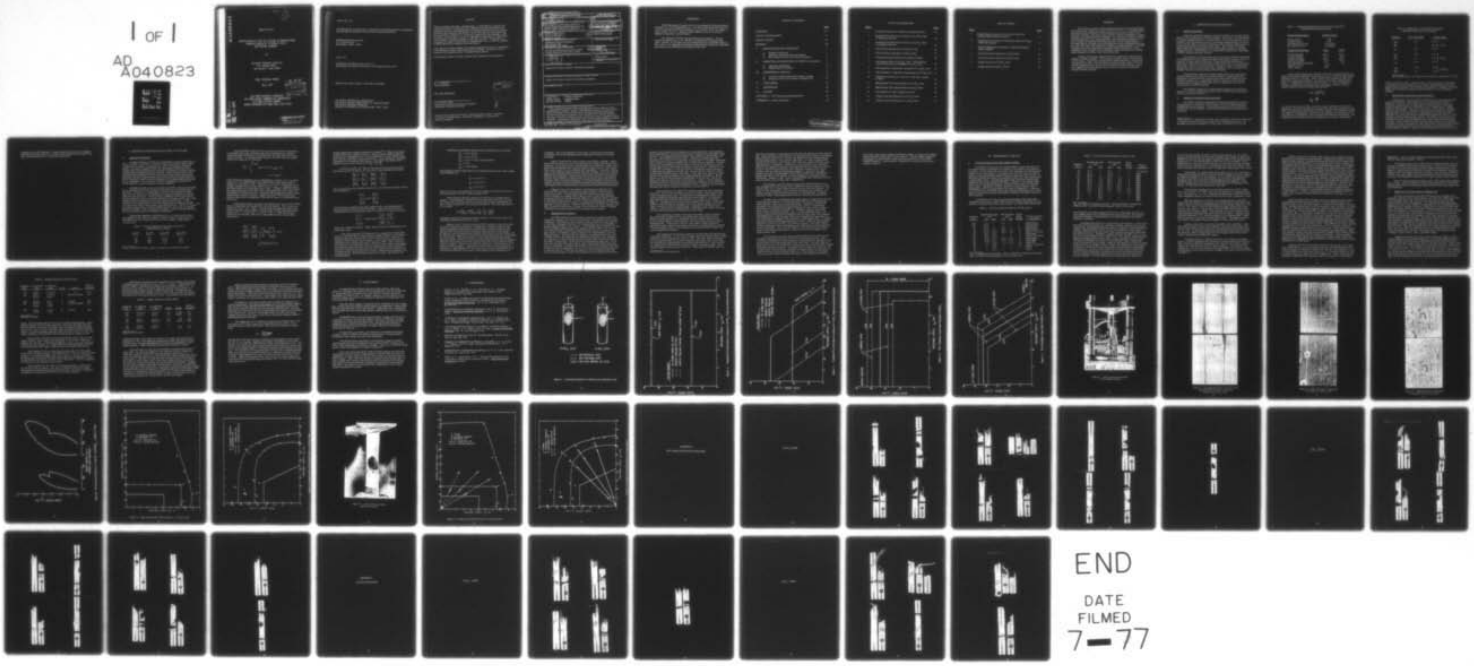

END
DATE FILMED
7-77

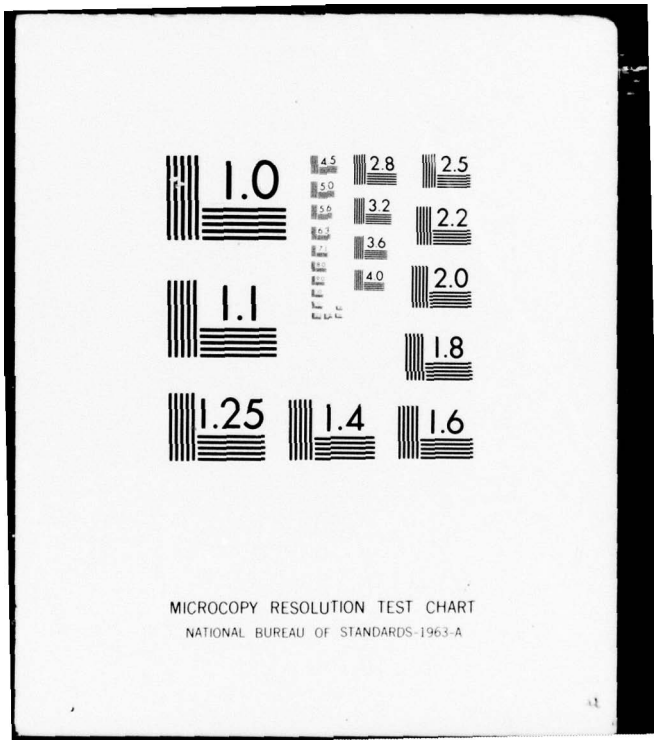
1.0
1.1
1.25
1.4
1.6
1.8
2.0
2.2
2.5
2.8
3.2
3.6
4.0
4.5
5.0
5.6
6.3
7.1
8.0
9.0
MICROCOPY RESOLUTION TEST CHART
NATIONAL BUREAU OF STANDARDS-1963-A

ADA040823

AFML-TR-77-62

INVESTIGATION OF FIRST PLY FAILURE IN GRAPHITE/EPOXY LAMINATES SUBJECTED TO BIAXIAL STATIC AND FATIGUE LOADINGS

By

SOUTHWEST RESEARCH INSTITUTE
P.O. DRAWER 28510
SAN ANTONIO, TEXAS 78284

FINAL TECHNICAL REPORT

APRIL 1977

DDC
RECEIVED
JUN 21 1977
A

AIR FORCE MATERIALS LABORATORY
AIR FORCE WRIGHT AERONAUTICAL LABORATORIES
AIR FORCE SYSTEMS COMMAND
WRIGHT-PATTERSON AIR FORCE BASE, OHIO 45433

AD No.
DDC FILE COPY

DISTRIBUTION STATEMENT A
Approved for public release;
Distribution Unlimited

AFML-TR-77-62

INVESTIGATION OF FIRST PLY FAILURE IN GRAPHITE/EPOXY LAMINATES SUBJECTED TO BIAXIAL STATIC AND FATIGUE LOADINGS

Southwest Research Institute
P. O. Drawer 28510
San Antonio, Texas 78284

April 1977

TECHNICAL REPORT AFML-TR-77-62
Final Report for Period 15 February 1975 through 15 March 1977

Approved for public release, distribution unlimited.

AIR FORCE MATERIALS LABORATORY
AIR FORCE WRIGHT AERONAUTICAL LABORATORIES
AIR FORCE SYSTEMS COMMAND
WRIGHT-PATTERSON AIR FORCE BASE, OHIO 45433

NOTICE

When Government drawings, specifications, or other data are used for any purpose other than in connection with a definitely related Government procurement operation, the United States Government thereby incurs no responsibility nor any obligation whatsoever: and the fact that the Government may have formulated, furnished, or in any way supplied the said drawings, specifications, or other data, is not to be regarded by implication or otherwise as in any manner licensing the holder or any other person or corporation, or conveying any rights or permission to manufacture, use, or sell any patented invention that may be related in any way thereto.

This report has been reviewed by the Information Office (IO) and is releasable to the National Technical Information Service (NTIS). At NTIS, it will be available to the general public, including foreign nations.

This technical report has been reviewed and is approved for publication.

N. J. PAGANO
Project Engineer

FOR THE DIRECTOR

S. W. TSAI, Chief
Mechanics and Surface Interactions Branch
Nonmetallic Materials Division

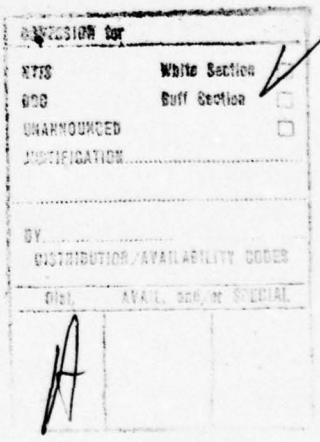

Copies of this report should not be returned unless return is required by security considerations, contractual obligations, or notice on a specific document.

UNCLASSIFIED

SECURITY CLASSIFICATION OF THIS PAGE (When Data Entered)

REPORT DOCUMENTATION PAGE	READ INSTRUCTIONS BEFORE COMPLETING FORM
1. REPORT NUMBER: AFML-TR-77-62	2. GOVT ACCESSION NO. / 3. RECIPIENT'S CATALOG NUMBER
4. TITLE (and Subtitle): Investigation of First Ply Failure in Graphite/Epoxy Laminates Subjected to Biaxial Static and Fatigue Loadings,	5. TYPE OF REPORT & PERIOD COVERED: Final Technical Report. 15 Feb 1975 - 31 March 1977 / 6. PERFORMING ORG. REPORT NUMBER: None
7. AUTHOR(s): Philip H. Francis, David E. Walrath, Donald N. Weed	8. CONTRACT OR GRANT NUMBER(s): F33615-75-C-5115
9. PERFORMING ORGANIZATION NAME AND ADDRESS: Southwest Research Institute, 8500 Culebra Rd, San Antonio, Tx 78284	10. PROGRAM ELEMENT, PROJECT, TASK AREA & WORK UNIT NUMBERS
11. CONTROLLING OFFICE NAME AND ADDRESS: Air Force Materials Laboratory/MBM, Wright-Patterson AFB, Ohio 45433	12. REPORT DATE: June 1976 / 13. NUMBER OF PAGES: 55 + Prelims
14. MONITORING AGENCY NAME & ADDRESS (if different from Controlling Office): 64p.	15. SECURITY CLASS. (of this report): Unclassified / 15a. DECLASSIFICATION/DOWNGRADING SCHEDULE

16. DISTRIBUTION STATEMENT (of this Report)

Approved for public release: distribution unlimited

17. DISTRIBUTION STATEMENT (of the abstract entered in Block 20, if different from Report)

Approved for public release; distribution unlimited

18. SUPPLEMENTARY NOTES

19. KEY WORDS (Continue on reverse side if necessary and identify by block number)

composites
biaxial loading
first ply failure
tubular specimens
graphite/epoxy
fatigue

20. ABSTRACT (Continue on reverse side if necessary and identify by block number)

Thin graphite/epoxy $[0/90]_s$ and $[\pm 45]_s$ tubes were loaded in various combinations of tension, torsion, and internal pressure, and physical evidence of first ply failure (FPF) was found using replication techniques. The FPF envelopes so identified were compared with ultimate strength envelopes, and with lamination theory predictions using a maximum strain criterion. Preliminary experiments were performed to examine the consequences of fatigue cycling inside of, and across the FPF envelope.

DD FORM 1 JAN 73 1473 EDITION OF 1 NOV 65 IS OBSOLETE

Unclassified

SECURITY CLASSIFICATION OF THIS PAGE (When Data Entered)

328 200

FOREWORD

This Final Report presents the work accomplished during the period February 15, 1975 through March 15, 1977 under USAF Contract F33615-75-C-5115 by Southwest Research Institute, P.O. Drawer 28510, San Antonio, Texas 78284. Dr. N. J. Pagano (AFML/MBM) served as the Project Engineer during this research effort.

Dr. Philip H. Francis was the SwRI project manager. He was closely assisted by Mr. D. E. Walrath in supervising the experimental work, and Mr. D. N. Weed, who was responsible for all specimen fabrication. Mr. F. S. Campbell developed the experimental testing and replication procedures, and conducted the mechanical test work.

TABLE OF CONTENTS

PRECEDING PAGE BLANK-NOT FILMED

LIST OF ILLUSTRATIONS

LIST OF TABLES

SUMMARY

This report presents results obtained primarily since the publication of the first annual report on contract F33615-75-C-515.[1] Two experimental procedures were developed for determining first ply failure (FPF) on the outer ply of $[0/90]_s$ and $[\pm 45]_s$ tubes loaded in various combinations of axial, torsional, and internal pressure loadings. One of these procedures, fluorescent dye penetrant, was soon abandoned as the replication technique proved more reliable in detecting FPF phenomena early in the loading history. First ply failure envelopes were determined for the two aforementioned four ply, thin wall tubes, and compared to ultimate strength envelopes. The FPF envelopes also were compared to lamination theory predictions, using a maximum strain criterion and accounting for initial stresses due to curing; these comparisons showed rather good agreement.

Finally, preliminary experiments were conducted to determine the influence of FPF on fatigue. Three groups of fatigue tests were conducted on both layups, along various proportional biaxial load paths. Each group consisted of two tests, both subjected to the same stress range, but in one test the maximum cyclic stress was held within the FPF envelope, and in the companion test the maximum cyclic stress was allowed to penetrate through the FPF envelope.

I. INTRODUCTION AND BACKGROUND

A. Research Objectives

Angle ply laminated composite materials exhibit very complex failure patterns when loaded beyond ultimate strength, and therefore the development of reliable strength theories is a difficult task. The overall objective of the present research program has been to investigate experimentally the threshold of local ply failure, when the first ply (or plies) begins to develop microcracks in the matrix under quasi-static loads. This concept of first ply failure (FPF) has been proposed as a possible physical basis for laminate strength theories, and therefore it is of interest to examine the relationship of FPF to ultimate laminate strength.

The first goal of this program was to develop an experimental method for detecting FPF on thin-walled laminated tubes loaded in-plane. This was achieved by using replica techniques, which limited the investigation to those stress states which would produce FPF on the outer ply. Using optical microscopy, however, it was possible to identify the onset of matrix shear and tensile cracks in $[0/90]_s$ and $[\pm 45]_s$ laminates, and to correlate these findings with theoretically predicted FPF envelopes.

Following this, exploratory biaxial fatigue tests were conducted to evaluate whether cycling across the FPF envelope is significantly more deleterious to fatigue life than cycling at the same stress range but within the FPF envelope. If, as postulated, FPF is a measure of irreversible microstructural damage, fatigue life should be affected in some way by cycling across the FPF threshold.

The detailed analytical and experimental findings are presented in Sections II and III, respectively, of this report, and the major conclusions drawn are set forth in Section IV.

B. Summary of Material Characterization

All tubular specimens manufactured and tested during the course of this program were fabricated with Fiberite hy-E 1034C high-temperature graphite/epoxy prepreg tape. This prepreg system uses Union Carbide's T-300 fiber, and is certified to meet the following Fiberite property specifications:*

*These data were obtained by Fiberite from composites which were fabricated by standard autoclave techniques using 100 psi augmented pressure. All strength values are reported in $\times 10^3$ psi units, all moduli are $\times 10^6$ psi.

Table 1. Fiberite Specifications for hy-E 1034C (T300/934) Graphite/Epoxy Material System

Prepreg Specifications	Nominal Values	
Resin Content	40%	
Volatile Content	0.5%	
Ply Thickness (cured)	.005 inches	
Gel Time at 340°F	11 minutes	
Composite Properties	**75°F**	**350°F**
Tensile Strength	235.0	200.0
Tensile Modulus	23.5	23.5
Flexural Strength	270.0	220.0
Flexural Modulus	23.0	23.0
Short Beam Shear Strength	16.0	9.5
Specific Gravity	1.60	
Fiber Volume	65%	

Early in the program this material system was characterized for its elastic and strength properties by testing $[0°]_4$ tubes, loaded by axial tension, internal pressure, or torsion. These results were compared to data developed from coupon type specimens, the results of which are summarized in Table 2. Complete test results are given in Ref. 1. Shear strengths and moduli were obtained from coupon tests using Rosen's analysis of [±45] coupons together with the following expressions:(2)

$$G_{xy} = \frac{\sigma_x}{2(\epsilon_x - \epsilon_y)}$$

$$S_{xy}^{us} = \frac{S_x^{ut}}{2}$$

As can be seen from the table, measured elastic coefficients are in close agreement, but some discrepancy is noted in the transverse strength of $[0°]_4$ tubes as compared to tensile tests of $[90°]_8$ coupons. Thin walled [0°] tubes are difficult to manufacture, and these lower strengths are probably due to a fine network of longitudinal cracks formed during specimen fabrication. The fragility problem in thin wall tubes disappeared, of course, when testing

Table 2. Comparison of Average Ply Properties Measured Using Tubes and Coupons*

Property	$[0°]_4$ Tube Data	Coupon Data	
E_{xx}	19.3	23.0	$[0°]_6$
S_x^{ut}	--	214	
ν_{xy}	0.35	0.34	
E_{yy}	1.44	1.6	$[90°]_8$
S_y^{ut}	3.5	6.8	
ν_{yx}	0.03	0.03	
G_{xy}	0.94	0.87	$[\pm(\mp)45]_s$
S_{xy}^{us}	11.1	10.8	

*All strength values are reported in ksi units, all moduli are 10^3 ksi.

$[0/90]_s$ and $[\pm 45]_s$ tubes. Although these cross-plied tubes are fabricated in essentially the same manner as $[0°]$ tubes, hoop stiffening due to fiber support greatly increases the durability of the specimen, making cross-plied tubes less susceptible to damage during fabrication or from subsequent handling.

C. Early Efforts at First Ply Failure Detection

Initial efforts at first ply failure detection were made using acoustic emission monitoring. The system has been previously described.(1) Basically, it made use of two piezoelectric ceramic PZT-5 transducers employing spatial filtering to eliminate noise not originating in the gage section of the specimen. Two tests were run on $[0/90]_s$ tubes, loading to failure in axial tension. Although acoustic emission activity was noted at approximately 50 ksi axial stress, no quantitative measurements were obtained, as acoustic activity did not take place between the sensors. Both specimens failed outside the gage section. All modes of first ply failure encountered in this research program were matrix-induced (either tension or shear). The Fiberite 934 epoxy prepreg resin system used in specimen fabrication is quite viscoelastic at room temperature, and the acoustic energy released during initial matrix crack development is presumed small and proved difficult to detect. Although acoustic emission may yet prove to be a

valuable tool for FPF detection, it was decided at that point to investigate alternative detection methods. All FPF measurements in this report were made with dye penetrants or replication microscopy.

II. PREDICTION AND DETECTION OF FIRST PLY FAILURE

A. Analytical Predictions

A simple analytical scheme was implemented to enable predictions of FPF to be made for balanced, symmetric angle ply laminates under states of plane stress loading. No attempt was made to develop new analytical models, but rather to establish how well conventional lamination theory coupled with an appropriate failure criterion can foretell the onset of FPF as as determined by experimental observations. Aside from its value in testing theoretical predictions of FPF, the model also was used to guide load selections during the experimental portion of the project to insure that FPF did not develop on interior plies inaccessable to the experimental techniques used. Additionally, the model was useful in evaluating the sensitivity of of FPF behavior to small variations in input quantities.

Lamination theory is now an accepted and widely used analysis/design tool in composite structures technology, and need not be reviewed here in any detail. However, it is important to include in the analysis the initial state of stress induced in each laminae of an angle ply laminate by cooling down from the cure cycle. These stresses originate from the anistropy of thermal expansion and the constraint afforded by contiguous plies, and result in tensile stresses tranverse to the fiber direction in each ply. These stresses can be estimated from macromechanical theory using the concept of a stress free state at some stress free temperature T_s, where $T_s < T_{cure}$. (3-5) The initial stresses thus calculated depend upon the cure cycle, the thermophysical properties of the composite ply material, and the stacking sequence, and can in certain cases be of significant magnitude.

The thermal expansion coefficients α_i $(i = 1, 2)$ were derived from data supplied by the material supplier, Fiberite Corp.[6] These data were provided in the form of average values $\bar{\alpha}_i$ over a range of temperatures $T_1 \leq T \leq T_2$*:

Table 3. Thermal Expansion Properties of T300/934 Graphite/Epoxy Laminae

T_1(°F)	T_2 (°F)	$\bar{\alpha}_1$ ($\times 10^6$)	$\bar{\alpha}_2$ ($\times 10^6$)
-65	+67	0.18	13.1
+67	+260	0.54	16.9
+67	+358	0.62	17.5

*$\bar{\alpha}_1$ is in the fiber direction and $\bar{\alpha}_2$ is transverse to the fiber direction.

As the laminate cools from the cure cycle full thermal contraction is prevented due to the constraint imposed by adjoining plies, with the result that tensile stresses are introduced into the plies transvers to the fiber directions. To calculate these stresses, first the vector of thermal strains of a single ply is calculated:

$$(\epsilon_i^T) = \int_{T_s}^{T_{room}} \alpha_i(T)\, dT = \bar{\alpha}_i\, (T_{room} - T_s)$$

$$i = 1,\ 2;\ \alpha_{12} = 0$$

If the functional dependence of α_i on temperature is known, e.g., as a polynomial in T, this relationship can be substituted directly into the above integral for evaluation of (ϵ_i^T). Otherwise, $\alpha_i\,(T)$ can be represented by an average constant value $\bar{\alpha}_i$ on the interval $[T_s,\ T_{room}]$, as suggested above, with little effect on the calculated value of (ϵ_i^T). In either event, the calculation depends directly on the value of T_s, the temperature (at or below cure temperature) at which the resin is considered to be sufficiently rigid to introduce thermal restraint stresses. Pagano and Hahn[3] have shown that a laminate under cure is essentially stress free at some T_s considerably less than T_{cure}.

In the present work, the stress free temperature was chosen as 250°F, based on experience with the Fiberite 934 resin system. Thus, in the calculations to follow $\Delta T = -180°F$. Averaged thermal expansion data $\bar{\alpha}_i$ were chosen from data shown in Table 3; these values resulted in thermal strain values of $\epsilon_1^T = -9.7 \times 10^{-4}$; $\epsilon_2^T = -3.0 \times 10^{-3}$; $\gamma_{12}^T = 0$. Specimen loading referred to the specimen axes) due to differential thermal cooling can be calculated as

$$t \begin{bmatrix} \sigma_x^T \\ \sigma_y^T \\ \tau_{xy}^T \end{bmatrix} = \begin{bmatrix} N_x^T \\ N_y^T \\ N_{xy}^T \end{bmatrix} = \int_z \int_T (\bar{Q})_k \begin{pmatrix} \alpha_x \\ \alpha_y \\ \alpha_{xy} \end{pmatrix}_k dT\, dz$$

$$= \int_z (\bar{Q})_k (T)_k^{-1} (\epsilon^T)\, dz$$

In these expressions standard notation is followed[7, 8]: $(\bar{Q})_k$ are the transformed reduced ply stiffness matrices, $(T)_k$ the transformation matrices carrying (x, y) components over to (1, 2) components, t is the laminae thickness, and the subscript k denotes the k^{th} ply. z is the thickness coordinate referenced to the midplane (see Figure 1). The above calculation yields negative values for the curing forces N_x^T, N_y^T, N_{xy}^T.

The ply forces $\bar{N}_x$, $\bar{N}_y$, $\bar{N}_{xy}$ are the sum of the curing forces calculated above and the forces N_x, N_y, N_{xy} due to direct mechanical loading:

$$\begin{bmatrix} \bar{N}_x \\ \bar{N}_y \\ \bar{N}_{xy} \end{bmatrix} = \begin{bmatrix} N_x \\ N_y \\ N_{xy} \end{bmatrix} + \begin{bmatrix} N_x^T \\ N_y^T \\ N_{xy}^T \end{bmatrix} = t \begin{bmatrix} \bar{\sigma}_x \\ \bar{\sigma}_y \\ \bar{\tau}_{xy} \end{bmatrix}$$

Then, using the laminate stiffness matrix [A], the laminate midplane strains are calculated by

$$\begin{bmatrix} \epsilon_x \\ \epsilon_y \\ \gamma_{xy} \end{bmatrix} = [A]^{-1} \begin{bmatrix} \bar{N}_x \\ \bar{N}_y \\ \bar{N}_{xy} \end{bmatrix}$$

The strains thus calculated are with respect to the cure temperature ply state as being the natural (unstrained) state. These strains are easily transformed over to the material frame of reference (1, 2) axes as follows:

$$\begin{bmatrix} \epsilon_1 \\ \epsilon_2 \\ \gamma_{12} \end{bmatrix}_k = [R][T]_k[R]^{-1} \begin{bmatrix} \epsilon_x^o \\ \epsilon_y^o \\ \gamma_{xy}^o \end{bmatrix} - \begin{bmatrix} \epsilon_1^T \\ \epsilon_2^T \\ 0 \end{bmatrix}$$

where [R] is Reuter's matrix. Again, these strains are referenced to the stress free state.

The remaining step in the analysis is to compute the stresses and strains in each ply under a given laminate loading condition, and compare these stresses and strains to their critical values (failure criterion) to determine FPF laminate load envelopes. In the work described here the maximum strain criterion was used to determine FPF. This criterion is very similar to the maximum stress criterion in that neither accomodates any interaction between strain (stress) components to influence failure.[8] The strain criterion was chosen because it is somewhat more sensitive to nonlinear stress-strain states than is stress, although this argument is not a compelling one. Secant modulus values were used, referenced to the strain at failure.

Individual ply properties used in these calculations are as follows:

$$E_{11} = 19.5 \times 10^6 \text{ psi}$$
$$E_{22} = 14.6 \times 10^6 \text{ psi}$$
$$G_{12} = 0.52 \times 10^6 \text{ psi (secant modulus)}$$
$$\nu_{12} = 0.35$$
$$t_{ply} = 0.005 \text{ inches.}$$

The following critical strain data for the unidirectional ply were used, drawn from Reference (1):

$$\epsilon_1^f = 9.30 \times 10^{-3}$$
$$\epsilon_2^f = 4.25 \times 10^{-3}$$
$$\gamma_{12}^f = 2.03 \times 10^{-2}$$

These values are room-temperature failure strains as determined from unidirectional tubular and flat coupon specimen tests.

The analytical approach required the inclusion of a simple search scheme. The laminate is considered to be loaded with some forces $\underline{P}$, and the critical ply and failure mode is sought by searching all combinations of failure modes and plies for the critical combination. The following calculation is made:

$$\chi = \underset{n \text{ plies}}{\text{Max}} \left\{ \underset{3 \text{ modes}}{\text{Max}} \left(\frac{\epsilon_1}{\epsilon_1^f}, \frac{\epsilon_2}{\epsilon_2^f}, \frac{\gamma_{12}}{\gamma_{12}^f} \right) \right\}$$

Assuming proportional loading and elastic behavior, the critical load corresponding to predicted FPF is $P_{cr} = P/\chi$.

Figures 2 and 3 show the predicted FPF envelopes on the outer plies for $[0/90]_s$ and $[\pm 45]_s$ specimens, respectively, having the stiffness and thermal properties given earlier and subjected to combined states of axial and torsional stress with internal pressure (hoop stress) as a parameter. In Figure 2, the horizontal lines represent matrix tension failure modes, and the vertical lines represent in-plane matrix shear failures and are not affected by hoop loading. Fiber tensile failure is not a predicted FPF mechanism. Note that internal pressure raises the predicted axial failure load; the Poisson effect provides greater axial load capacity before the critical matrix tensile strain is reached. Figure 2 also shows the influence of curing strains on the predicted FPF envelopes. Accounting for these initial strains reduces the envelopes by approximately 16 %; the shear failure mode is independent of the curing strain influence in this case, as the material and loading axes are

coincident. Due to the symmetry of the layup, the axial and hoop stress coordinates can be interchanged without affecting the location of the FPF envelopes.

Figure 3 presents the same results for the $[\pm 45]_s$ laminate. Again, axial and hoop values can be interchanged without change to the figure due to symmetry. In the $[\pm 45]_s$ case, the horizontal lines represent in-plane shear failure and the diagonal lines represent matrix tensile failure. Here again, fiber tensile failure is not a predicted FPF mechanism. As before, accounting for cure-induced strains contracts the FPF envelope in the sense that the diagonal lines (tension failures) move inward but the horizontal lines (shear failures) are unchanged. Unlike the previous case, however, here internal pressure hoop stress does influence the in-plane shear region of the failure envelope. This is so since the material (1, 2) and the loading (x, y) axes are not aligned, and hence the transverse matrix tensile strain ϵ_2 depends directly on all three applied stress components $\sigma_x, \sigma_y, \tau_{xy}$ through the transformation equations.

Figures 4 and 5 are presented to illustrate the sensitivity of the predicted FPF envelopes to the input thermal expansion coefficient and failure strain data. In these figures the FPF envelope for axial tension/torsion loadings are repeated from Figures 2 and 3, and ±10% variations are given first to the average thermal expansion coefficient data $\bar{\alpha}_i$, and then to the matrix failure strains. As can be seen the envelopes are expected to be much less sensitive to variations in average thermal expansion coefficient data than to failure strains. Both the matrix tension and shear regions of the FPF envelope are affected by changes in the input failure strains, although variations in $\bar{\alpha}_i$ make no difference on the shear failure modes.

B. Experimental Procedures

Two FPF methods were developed to acquire the experimental data during this program: fluorescent dye penetrant, and replication microscopy techniques. Both methods were limited to failure detection on the outer ply of the tubular specimen, therefore all loading sequences were designed to produce expected FPF in the outer ply. The experimental procedure involved first thoroughly examining the outer specimen surface under zero load for any cracks that may be present, using fluorescent dye in one region of the gage section, and making a plastic replica of the complementary region of the gage section. Then the tube was loaded to a predetermined level, then reduced while the dye penetrant and replication techniques were reapplied. All replicas for a given test specimen were made while the load was held at the same constant value, which was 50% of the predicted FPF load. On the first cycle the specimen was loaded to 50% of the predicted FPF load, then held for replication, unloaded and reloaded to 60% of the predicted FPF load, dropped to 50% for replication, and so on in 10% increasing load increments to specimen failure. The load was reduced to 50% of predicted FPF load prior to acquiring data records with the penetrant and replication techniques

because of the tendency of the specimen to creep under load, which tended in early experiments to cause the matrix cracks to extend during the data-taking process. By dropping the load somewhat crack extension was inhibited, yet the cracks still remained partially open. When the dye examination and replication procedures were completed, the specimen was unloaded completely, then reloaded to a higher maximum load, and the process repeated. This procedure was continued until ultimate failure of the entire specimen occurred. All specimens were tested under conditions of load control. Testing was conducted under conditions of load rate control, whereby the internal pressure or axial load was applied at a fixed rate, and the torsional load was coupled in accordance with the stress vector path. Load rates were chosen for each test so as to produce maximum load in approximately two minutes. Stress rates $\dot{\sigma}_y$ for the $[0/90]_s$ tube tests varied from 66-365 psi/sec, and for the $[\pm 45]_s$ tube tests $\dot{\sigma}_x$ varied from 66-329 psi/sec. Figure 6 shows a tubular specimen mounted in the biaxial loading facility; particulars on the tube fabrication process may be found in References 1 and 9. Details of the fluorescent dye penetrant and the replication procedures are given below.

Fluorescent dye was applied by wiping the specimen with a saturated gauze pad. The dye was allowed to set for five minutes, then wiped off with a water-dampened gauze pad. The specimen was photographed under ultraviolet illumination using high speed film and yellow filters. An example of FPF detected with fluorescent dye penetrant in a $[0/90]_s$ tube is shown in Figure 7. Although the dye could be used to detect FPF cracks, it was often difficult to discriminate an emergent crack from general background visual "noise" caused by surface irregularities. Replication techniques proved superior to penetrants for detecting FPF at somewhat lower loads, therefore the use of dye penetrants was abandoned for later tests.

Two replicating systems were tried on the tubes: acetyl cellulose tape with methyl acetate solvent, and acetate tape with acetone solvent. Previous SwRI experience on replicating cracks in metals had shown the acetyl cellulose/methyl acetate system to be easier to use, due to a shorter hardening time. It was found, however, that methyl acetate chemically attacked the epoxy matrix of the tubular specimens, causing surface marring. To avoid damage caused by the replication, the acetate/acetone system was used throughout this program.

The loading and observation sequences were the same for both dye and replication techniques. At zero load, a replica was taken of the center 3 inches of the tube using a acetate strip one inch wide. Thus, the region of replication covered the center three inches along the tube length, and 1 inch around the circumference (approximately one-third around the tube). This was done by coating the acetate tape with acetone, partially softening the tape, which was then applied to the surface of the tube. After about 10 minutes when the

*Uresco tracer tech penetrant.

tape had rehardened, it was peeled from the tube and labeled for later observation. After the baseline observations, the specimen was loaded to successively higher predetermined values, but the load reduced and held constant during the replication process, as previously described. In order to examine the replica records under a microscope, they were first coated with a thin vapor deposited layer of aluminum. Replicas for each specimen were examined with a stereo-optical microscope, beginning with the last replica just before fracture, and working backwards in the replication sequence until cracks present in the last replica disappeared altogether. In this way an upper bound on the load corresponding to FPF could be established. Photomicrographs were taken of all replicas in which emergent or developed cracks were found. Figures 8 and 9 show cracks detected with replication microscopy of a $[\pm 45]_s$ and a $[0/90]_s$ tube, respectively.

The technique just described presumes that FPF develops more or less homogeneously over the ply under conditions of uniform stress, so that records taken over a small region characterize the entire ply behavior. In order for this assumption to be valid under laboratory test conditions, the tubular specimen must have high tolerances of wall thickness, roundness, and fiber volume, and the gage section must be isolated from grip effects.

All tubes were instrumented with strain gages to obtain strain records during the load sequence. It was thought that these curves might provide some indication of the onset of first ply failure. Although no useful FPF correlates were obtained from these hysteresis curves, an interesting phenomenon was noted when the applied loading on a tube caused in-plane shear stress on the outer laminae, i. e., torsional loading of the $[0/90]_s$ tubes or axial loading of the $[\pm 45]_s$ tubes. As described previously, the loading sequences consisted of loading the tube to some level, then reducing and holding load at some constant value while replicating the specimen surface, followed by unloading, and reloading to a higher peak value. A constant load hold normally lasted approximately 8 minutes. Figure 10 shows typical hysteresis curves for a $[0/90]_s$ tube loaded in torsion. The initial linearly elastic component of the strain response was subtracted out electronically to increase resolution. Thus, had the material been ideally linearly elastic a cycle of load would have produced a strain record that would appear as a single vertical line.

It is of interest to notice that just past the peak load of both curves the strain continued to increase even as the load was decreasing. This "overshoot" phenomenon is characteristic of creep behavior, enhanced in the present case by the low stress rate (66 psi shear/sec). At lower values of peak load (curve on left in Figure 10) creep occurred as load was held constant during the replication process. At higher values of peak load, however, the creep process reversed itself, and strain decreased under constant load, as shown in the curve on the right in Figure 10. This sequence of creep and "reverse creep" events was found consistently in the testing of both $[\pm 45]_s$

and $[0/90]_s$ tubes during uniaxial and biaxial loading, so long as one loading mode produced in-plane shear on the outer ply. During loading sequences producing no in-plane shear, strain records showed only a very slight anelastic behavior, as the material responded in a basically linear elastic manner to failure.

III. EXPERIMENTAL RESULTS

A. First Ply Failure Under Quasi-Static Loading

To measure first ply failure experimentally, tubular specimens of two different fiber orientations were loaded in incremental load sequences to failure. As was previously described, each specimen was loaded proportionally in the stress plane to some peak value, then the load was reduced (again, along a proportional path) and held at some lower value of load. At this time a replica was taken of the specimen surface for later examination to detect FPF cracks. Increasingly higher peak loads were applied until ultimate failure of the specimen resulted. A total of 27 quasi-static FPF tests were run during this program, thirteen $[0/90]_s$ tubes, and fourteen $[\pm 45]_s$ tubes. Summaries of these results are listed in Tables 4 and 5; photographs of the broken specimens are shown in Appendix A. Figures 11 and 12 show plots of the FPF and ultimate strength measurements in stress space as well as the predicted FPF failure envelopes developed using lamination analysis.

It should be clear that one of the shortcomings of the replication technique as used here to detect FPF is the fact that the specimen was subjected to as many as about ten cycles of load. It is quite likely that though

Table 4. First Ply Failure Results for $[0/90]_s$ Tubes

Specimen No.	Ultimate Strength (ksi) σ_y	Ultimate Strength (ksi) τ_{xy}	FPF Strength (ksi) σ_y	FPF Strength (ksi) τ_{xy}	Stress Ratio σ_y/τ_{xy}	Failure Location and Type
123	71.7	–	61.7	–	–	seam/tension
126	80.2	–	–	–	–	seam/tension
42	113.5	–	31.0	–	–	gage/tension
41	115.4	11.5	54.0	5.4	10	seam/tension
45	69.4	13.9	30.8	6.2	5	shear/1" from tab
44	48.2	15.9	–	–	3	shear/gage
18	31.0	15.5	–	–	2	shear/1" from tab
121	32.2	16.1	29.7	14.9	2	shear/gage
37	19.0*	19.0	17.9	17.9	1	shear/gage
124	7.7	15.4	7.4	14.9	1/2	shear/tab
43	3.7	14.8	–	–	1/4	shear/1" from tab
36	–	15.6	–	–	–	buckle
40	–	15.8	–	–	–	buckle

*σ_x, as loading was axial tension. From symmetry of loading and material axes, σ_y should be interchangable with σ_x in this case.

Table 5. First Ply Failure Results for $[\pm 45]_s$ Tubes

Specimen No.	Ultimate Strength (ksi) σ_x	Ultimate Strength (ksi) τ_{xy}	FPF Strength (ksi) σ_x	FPF Strength (ksi) τ_{xy}	Stress Ratio σ_x/τ_{xy}	Failure Location
48	25.5	–	19.0	–	–	1" from tab
32	31.2	–	29.5	–	–	gage
47	40.4*	–	34.5*	–	–	gage
119	32.0	5.3	31.9	5.3	6	gage
92	32.9	5.5	25.5	4.2	6	gage
96	38.2	9.6	32.9	8.2	4	gage
89	27.3	13.6	24.0	12.0	2	gage
106	31.8	31.8	29.7	29.7	1	gage
93	23.5	35.3	20.7	31.1	2/3	gage
88	13.3	39.9	11.7	35.2	1/3	gage
90	6.7	40.2	–	–	1/6	gage
52	–	35.3	–	–	–	gage
21	–	35.8	–	–	–	gage
107	–	41.6	–	–	–	gage

*σ_y, as loading was internal pressure. From symmetry of loading and material axes, σ_x should be interchangable with σ_y in this case.

few in number, the stress ranges involved were rather high and some low cycle fatigue effects may inadvertently have been produced. The extent to which this specimen cycling influenced the FPF thresholds found experimentally is unknown.

Looking first at Figure 11 for the $[0/90]_s$ test results, it can be seen that some of the data points are somewhat scattered, particularly along the vertical axis representing transverse stress σ_y imposed by internal pressure loading. Data presented in Table 4 have been organized to show points on the graph moving out from the origin, then clockwise around the graph from the vertical (σ_y) axis. Therefore, uniaxial ultimate strengths of 71.7, 80.2, and 113.5 ksi are listed for tube numbers 123, 126, and 42, representing the ultimate strength points on the σ_y axis, moving vertically from the origin. The failure envelopes were more or less arbitrarily drawn, taking into account the type of failure evident. Because tube numbers 123 and 126 failed along the spiral lap junction of the 90° plies, indicating possible fabrication deficiencies, these results were discounted (see the specimen photographs in Appendix A). Failure in tube number 42 occurred along a vertical line, not in the spiral lap junction, therefore this result was considered valid. All three specimen failures resulted from tension caused by the internal pressure loading. Two FPF data points were detected with replicas at

31.0 ksi for tube number 42 and 61.7 ksi for tube number 123. It is interesting to note the lowest recorded FPF strength under uniaxial σ_y stress was exhibited by the tube with the highest ultimate strength for this loading mode. Because the 61.7 ksi FPF strength of tube #123 is so much higher, it was thought the true first ply failure event may not have been a strongly dominant crack within the replicated area, and therefore may have been missed. The failure envelope was therefore drawn to weight lower FPF points more heavily.

Tube number 41, tested with a stress ratio $\sigma_y/\tau_{xy} = 10$, is the first biaxial point moving clockwise around the graph in Figure 11 from the vertical. An ultimate strength of 115.4 ksi tension, 11.5 ksi shear was measured for this tube, with failure occurring along the spiral seam of the (internal) 90 degree plies, as can be seen in the photograph in the Appendix. Final failure resulted from torsional stresses which sheared the specimen off at the tab. No FPF point was measured for this tube.

In-plane shear appeared to be the failure mode of tube #45, loaded with a σ_y/τ_{xy} ratio of 5. FPF cracks were detected after an applied stress of $\sigma_y = 30.8$ and $\tau_{xy} = 13.9$ ksi. Contrast the appearance of tube #45 with its many longitudinal cracks, to tube #42 with only one major longitudinal crack.

With the exception of two tubes, the remaining $[0/90]_s$ specimens tested with load ratios of increasing torsion showed failures with many longitudinal cracks, as shown in the photographs for the six tube numbers 44, 18, 121, 37, 124, and 43. Tube #37 was loaded with axial tension and torsion, along a σ_x/τ_{xy} ratio of 1; calculations indicated FPF would be due to shear caused by the torsional loading. Many vertical cracks were evident in the failed specimen indicating FPF was probably due to shear. Although a FPF point was detected at 17.9, this point appears to be somewhat high. Actual first ply failure was probably missed by the replica. The failure envelope was drawn in this region with more emphasis on the lower FPF points.

Failure of tube #121 occurred in the center of the specimen. Tabs were later cut away to make visual inspection under the microscope easier. Only two FPF points were measured for the aforementioned six tubes (Nos. 44, 18, etc.), as detecting cracks with replication during torsional loading was difficult. Shear cracks tended to be more tightly closed than tensile cracks, therefore more difficult to detect.

The final two tubes, numbers 36 and 40, were tested with uniaxial torsion. Failure apparently was caused by torsional buckling (see Figure 13). Upon removal of load these specimens both reverted back to their original shapes, and retained most of their original stiffness. This behavior was surprising, since earlier theoretical and experimental work with $[0]_4$ tubes showed them to have torsional failure strengths well below torsional buckling strengths. (1)

Of the 13 tests run on $[0/90]_s$ tubes, only 6 tests resulted in clearly detectable first ply failure measurements. Although these points do not fall exactly where predicted, the general agreement is fair and the shape of the failure envelope determined by four of the points does closely resemble the rectangular sharp-corner shape of the predicted FPF envelope. The biggest margin of error appears to be in placement of the right hand region of the predicted failure envelope, which is largely determined by the shear modulus of the material. The predicted FPF envelope was produced using a secant modulus value of $G_{12} = 5.5 \times 10^5$ psi to describe the in-plane laminae shear properties. One would expect that the "effective" shear modulus relevant to this type of approximate analysis would properly lie between the secant and tangent moduli for the ply failure strain γ_{12}, and indeed this conjecture was confirmed by varying the input parameters in the analysis. However, the purpose here was not to "curve fit" the predicted FPF envelope to the data, but rather to demonstrate that the computations based on measured ply properties and accounting for curing strains produce acceptable predictions of FPF behavior. It seems reasonable that improved predictions could be made using a nonlinear laminate analysis accounting for the true $\tau_{12} - \gamma_{12}$ relation.

First ply failure data for $[\pm 45]_s$ tubes were generated using various combinations of axial tension and torsion. Results listed in Table 5 are plotted in Figure 12 in the same manner as previously described for $[0/90]_s$ tubes. Points plotted along or near the vertical σ_x axis, as before, are quite scattered. This portion of the graph corresponds to in-plane shear failure in the material. The predicted FPF envelope is represented as a horizontal line in this region. Three tubes, numbers 48, 32, and 47 were tested under uniaxial stress: tubes 48 and 32 were tested with axial tension, while tube number 47 was tested with internal pressure loading. Results from tube number 47 have been included on this graph along with those from specimens 48 and 32 because the stress states in these specimens are the same, if tube curvature effects are discounted as small. Three FPF points were generated, ranging from 19.0 ksi for tube number 48 to 34.5 ksi for tube number 47. Ultimate strengths ranged from 25.5 ksi to 40.4 ksi. Many cracks along the fiber axis were noted on all three failed specimens (see Appendix A). Specimens tested to failure with axial tension did not exhibit failure features different than those specimens tested to failure with torsion. Visual evaluation could not verify that a $[\pm 45]_s$ tube failed due to in-plane shear rather than matrix tension, although laminate calculations of FPF should provide reliable predictions as to FPF mode.

Moving clockwise around the plot from the vertical axis, four tubes were tested with σ_x: τ_{xy} ratios greater than one, placing data points in the region predicted to represent in-plane shear failure. Tube numbers 119 and 92 were tested along a load ratio line $\sigma_x/\tau_{xy} = 6$, with tube numbers 96 and 89 tested along σ_x/τ_{xy} paths of 4 and 2 respectively. Again, data points are somewhat scattered so that locating the failure envelope is to some extent

judgemental. All four of these biaxial tests did produce FPF values found with the replication technique, however.

The remaining tubes were tested with increasing torsional load components, including 3 tubes tested in pure torsion. Tubes 106-107 inclusive (see Table 5) all were predicted to produce matrix tensile failures in the material. Data points for these tests are much less scattered, making estimation of failure envelopes much more reliable. Note, however, detection of FPF cracks with replicas during predominately torsional loading was not achieved, even though this predicted to be a matrix tensile mode of failure.

Out of 14 tests conducted on $[\pm 45]_s$ tubes, FPF results were obtained from 10 tests. First ply failure envelopes were estimated from these data, although some points corresponding to predominantly axial (σ_x) loading were quite scattered.

B. Influence of First Ply Failure on Fatigue Life

In order to determine what effect FPF may have on fatigue life of composite laminates under biaxial loading, six sets of two fatigue tests each were conducted, three sets of two tests on each layup used in the FPF characterization part of the program. The objective in conducting these fatigue tests was to learn whether cycling within the FPF envelope produces significantly less damage/cycle than cycling across or above the FPF envelope. The approach was to cycle a pair of identical specimens along a proportional load path; a constant value of σ_y/τ_{xy} for $[0/90]_s$ tubes and a constant σ_x/τ_{xy} for $[\pm 45]_s$ tubes. One member of the pair was to be cycled with a peak stress outside the FPF envelope, and the other specimen to be cycled entirely within the FPF envelope. The stress range was held constant for both members of specimens tested along a given stress vector, but the stress range did vary somewhat across specimen pairs due to the fact that the specimen failure envelope varied in proximity to the FPF envelope for the various stress vectors. Note also that while the stress range was fixed for specimen pairs, the "load ratio" R = minimum stress in cycle/maximum stress in cycle necessarily was different. All fatigue tests were conducted under conditions of load control, using a sinusoidal signal.

Fatigue test results for [0/90] tubes are shown in Table 6. Peak stress values have been plotted in Figure 14 , in which the experimental and analytical FPF results have been superimposed to show the stress ratios and the relationship of peak stress levels to the FPF envelope. Three stress ratios σ_y/τ_{xy} = 3, 5, and 10 (imposed by combined torsion and internal pressure) were conducted. Tube number 120 was cycled between σ_y = 20, τ_{xy} = 6.7 ksi and σ_y = 40, τ_{xy} = 13.3 ksi and failed after 4 cycles. Later examination of the replicas showed the tube had cracked during the first cycle of load. The second specimen, tube number 130, was cycled along the same stress path, but at a lower peak stress value with approximately the same stress

Table 6. Fatigue Results for $[0/90]_s$ Tubes

Specimen No.	σ_y max/min (ksi)	τ_{xy} max/min (ksi)	σ_y/τ_{xy}	Cycles	FPF on 1st Cycle
120	40/20	13.3/6.7	3	4	Yes
130	20/0.3	6.7/0.1	3	100,000 (runout)	No
	45.7*	15.2*			
122	50/25	10/5	5	11,061	Yes
127	25/1.0	5/0.1	5	113,000 (runout)	No
	66.6*	13.3*			
125	50/25	5/2.5	10	101,000	Yes
	75.8*	7.6*			

*Residual strength.

range. This specimen endured 10^5 cycles of loading without failing. In the interest of time, 10^5 cycles was defined as runout; the specimen was then loaded to failure along the same stress ratio recording a residual strength of $\sigma_y = 45.7$, $\tau_{xy} = 15.2$ ksi. No FPF crack was detected on the first cycle replica. All $[0/90]_s$ fatigue specimens were cycled at a rate of 0.5 Hz, this being a limitation of the machine when internal pressure loading is used.

Tube numbers 122 and 127 were cycled along a stress ratio of 5 with similar results. Tube number 122 failed after 11,061 cycles, while tube number 127 "ran out". A residual strength of $\sigma_y = 66.6$, $\tau_{xy} = 13.3$ ksi was recorded for tube number 127. Again, the tube cycled above FPF showed a crack on the first cycle replica while the tube cycled below FPF did not.

Tube number 125 was cycled along a stress ratio of 10 with a peak stress above the FPF envelope. This specimen also "ran out" and was tested to failure. A residual strength of $\sigma_y = 75.8$, $\tau_{xy} = 7.6$ ksi was recorded. Because a tube cycled below the FPF point would also be expected to runout, the second test was not run in order to save some time. To cycle a specimen 10^5 times at 0.5 Hz required over 55 hours.

Tube numbers 120, 122, and 127 all showed evidence of FPF following the first cycle of loading. This was to be expected since the loading was intended to exceed the measured FPF envelope, and serves to engender confidence in the measured FPF surface for $[0/90]_s$ laminates.

Axial tension and torsion were imposed on the six $[\pm 45]_s$ tubes tested in fatigue along stress paths of σ_x/τ_{xy} = 1/3, 2/3, and 1. These results are shown in Table 7, and the stress trajectories are plotted in Figure 15. As indicated by the Figure, the stress range the same for each member in a pair of specimens loaded along a common stress path. Testing rate was a problem for these tests, initially a cyclic rate of 5 Hz was used, but failure was found to be occurring on the first cycle. The decision was then made to

Table 7. Fatigue Results for $[\pm 45]_s$ Tubes

Specimen No.	σ_x max/min (ksi)	τ_{xy} max/min (ksi)	σ_x/τ_{xy}	Cycles	FPF on 1st Cycle
154	12.3/1.6	37/4.9	1/3	4,053	No
148	11/0.3	33/0.9	1/3	74,832	Yes
141	22/3.3	33/4.9	2/3	271	Yes
149	19/0.3	28.5/0.5	2/3	4,640	Yes
147	27/4.5	27/4.5	1	—	*
144	23/0.5	23/0.5	1	913	No

*Broke on first cycle

conduct the initial 10-20 cycles at a rate of 1 Hz, after which the rate was increased to 5 Hz. This approach eliminated problems with failure during the first cycle, but again demonstrates the strain rate dependence of this matrix material. None of the $[\pm 45]_s$ specimens survived 10^5 cycles.

First ply failure cracks were not detected as expected during any of these tests. No crack was detected on the replicas for tube number 154, which was cycled above the FPF envelope along the path σ_x/τ_{xy} = 1/3. A crack was detected, however, in tube number 148, which was tested at lower stress values. The FPF envelope had been considered to be well defined in this region of stress space, and for this reason peak stresses were chosen so as to cycle one tube just above and one just below the envelope. Perhaps the reversal of expected replication results stems from minor irregularities in the specimens which may have or may not have caused FPF outside the replication region in the case of specimen 154. Despite this apparent contradiction in FPF results, it is important to note that specimen 148, cycled at what might be considered to be below the FPF threshold, endured considerably more load cycles than specimen 154, cycled further into the FPF regime.

Replicas from both tubes tested on the stress ratio of 2/3 showed cracks, again indicating the exact position of the FPF envelope was not known. Rate effects may well have had some effect, as the loading rate used on the first cycle of fatigue loading (1 Hz), was different from that used during FPF measurement. Of the tubes tested along the stress ratio line of 1, tube number 147 broke on the first cycle. Tube number 144, tested at lower stress values, failed after 913 cycles and showed no FPF crack after the first cycle.

In summary, in five pair of tests where comparative fatigue lives could be determined, each showed the fatigue life to be considerably reduced when the stress range spanned the FPF limit as compared to a test at the same stress range but with the peak stress within the FPF limit. Undoubtably part of the reason for this can be attributed to the higher cyclic stresses in the former case. However, the decided contrast in the cyclic values suggests that part of the reason is due to microstructural damage induced in penetrating the FPF envelope.

The fatigue data can be examined in light of the accepted "S-N" relation $\sigma_{max} = AN^{-B}$ where σ_{max} is the maximum stress per cycle, N the cycles to failure at that cyclic stress, and A and B are positive constants. Then,

$$B = - \frac{d(\ell n\, \sigma_{max})}{d(\ell n\, N)}$$

showing that in this log-log linear relation B is the (negative of the) slope of the $\ell n\, \sigma$ vs. $\ell n\, N$ graph. Applying this fatigue relationship to each of the five pair of test data, the coefficient B is found to average about 0.045. This value is very nearly the same as established by SwRI in other program work for the cyclic fatigue behavior of the same material system having a circular hole. The coefficient B for unnotched tubes is much less, indicating that the effect of cycling across the FPF envelope as compared to cycling inside the envelope is approximately the same as a stress concentration factor of two or three. While this argument is far from conclusive, it does support the notion that FPF mechanisms aggravate fatigue life, over and above the effect of the stress level.

IV. CONCLUSIONS

An experimental technique using an acetate/acetone replicating plastic in conjunction with optical microscopy afforded a means of observing and measuring FPF cracking on the outer surface of tubular specimens maintained at constant load. By making a sequence of such replicas at successively higher load levels it is possible to determine retrospectively the onset of the FPF event.

First ply failure appears to develop rather uniformly over the critical ply, so that a three inch square replica usually was sufficient to capture FPF features characteristic of the entire surface. Difficulties were encountered in a relatively few cases where tube failure evidently was due to a fabrication defect.

Lamination theory incorporating the effects of initial stresses due to curing can be used to construct an analytical model of FPF that correlates reasonably well with observed FPF values. The model indicates that FPF predictions are relatively insensitive to the average thermal expansion coefficient data used as model input, but highly sensitive to the ultimate strain failure data used.

For the $[0/90]_s$ and $[\pm 45]_s$ G/E laminates investigated during this program, FPF was always due either a matrix shear or a matrix tension mechanism; fiber tension was not a FPF mechanism.

The ultimate failure envelope for G/E material samples loaded in combined axial and shear loading lies well outside the FPF envelope (from 15% to 400%; depending on the mode of loading). Therefore, structural design based on FPF would appear to be quite conservative.

The cyclic life of specimens loaded in biaxial fatigue was decreased considerably when the stress range spanned across the FPF threshold, as compared to loadings where the (same) stress range was entirely within the FPF envelope. This consistent decrease in fatigue life may be attributed in part to higher peak stresses encountered when crossing the FPF envelope, and in part to the micromechanical damage introduced when exceeding the FPF limit. The number of observations was insufficient to allow a more definite statement to be made.

V. REFERENCES

1. Francis, P. H., Walrath, D. E., and Week, D. N., "Strength Behavior of Graphite/Epoxy Laminates Under Biaxial Load," AFML-TR-76-86, July 1976.

2. Rosen, B. W., "A Simple Procedure for Experimental Determination of the Longitudinal Shear Modulus of Unidirectional Composites," Journal of Composite Materials, Vol. 6, No. 4 (October 1972), pp. 552-554.

3. "Curing Stresses in Composite Laminates," by H. T. Hahn and N. J. Pagano, Journal of Composite Materials, Vol. 9, 91-106 (January 1975).

4. "Evaluation of Composite Curing Stresses," by N. J. Pagano and H. T. Hahn, presented at ASTM 4th Conference on Composite Materials: Testing and Design, Valley Forge, PA, May 3-4, 1976.

5. "On the Hygrothermal Response of Laminated Composite Systems," by R. B. Pipes, J. R. Vinson, and T. W. Chou, Journal of Composite Materials, Vol. 10, 129-148 (April 1976).

6. Personal communication with Mr. Ed Himmelman, Fiberite Corp., Winona, MN, May 1976.

7. PRIMER ON COMPOSITE MATERIALS: ANALYSIS, by J. E. Ashton, J. C. Halpin, and P. H. Petit, Technomic Publishing Co., Inc., Stamford, 1969.

8. MECHANICS OF COMPOSITE MATERIALS, by R. M. Jones, McGraw-Hill Book Co., New York, 1975.

9. Weed, D. N., and Francis, P. H., "Process Development for the Fabrication of High-Quality Composite Tubes," Fibre Science and Technology (in press).

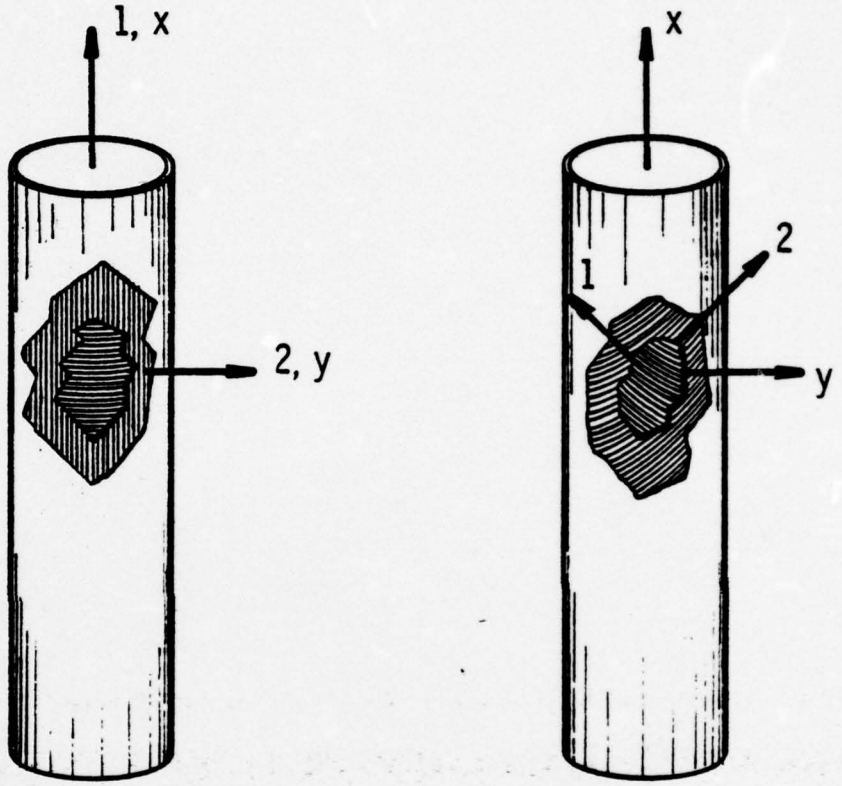

$[0/90]_S$ LAYUP

$[\pm 45]_S$ LAYUP

(1, 2) ARE MATERIAL AXES
(x, y) ARE SPECIMEN AXES
3 and z ARE AXES NORMAL TO PLIES

Figure 1. Coordinate Systems for Material and Specimen Axes

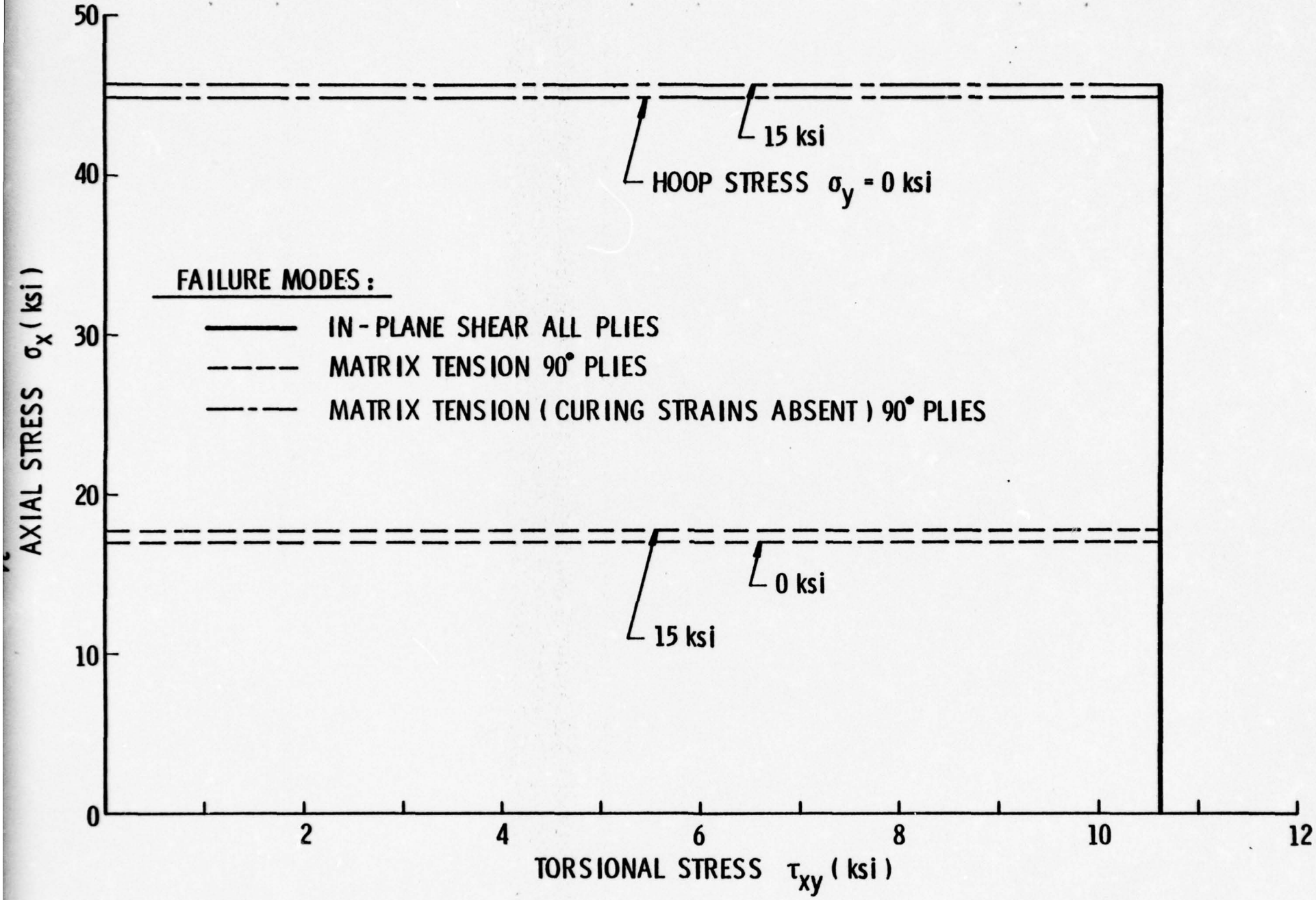

Figure 2. Predicted First Ply Failure Surfaces of $(0/90)_s$ Tubes by Laminate Analysis

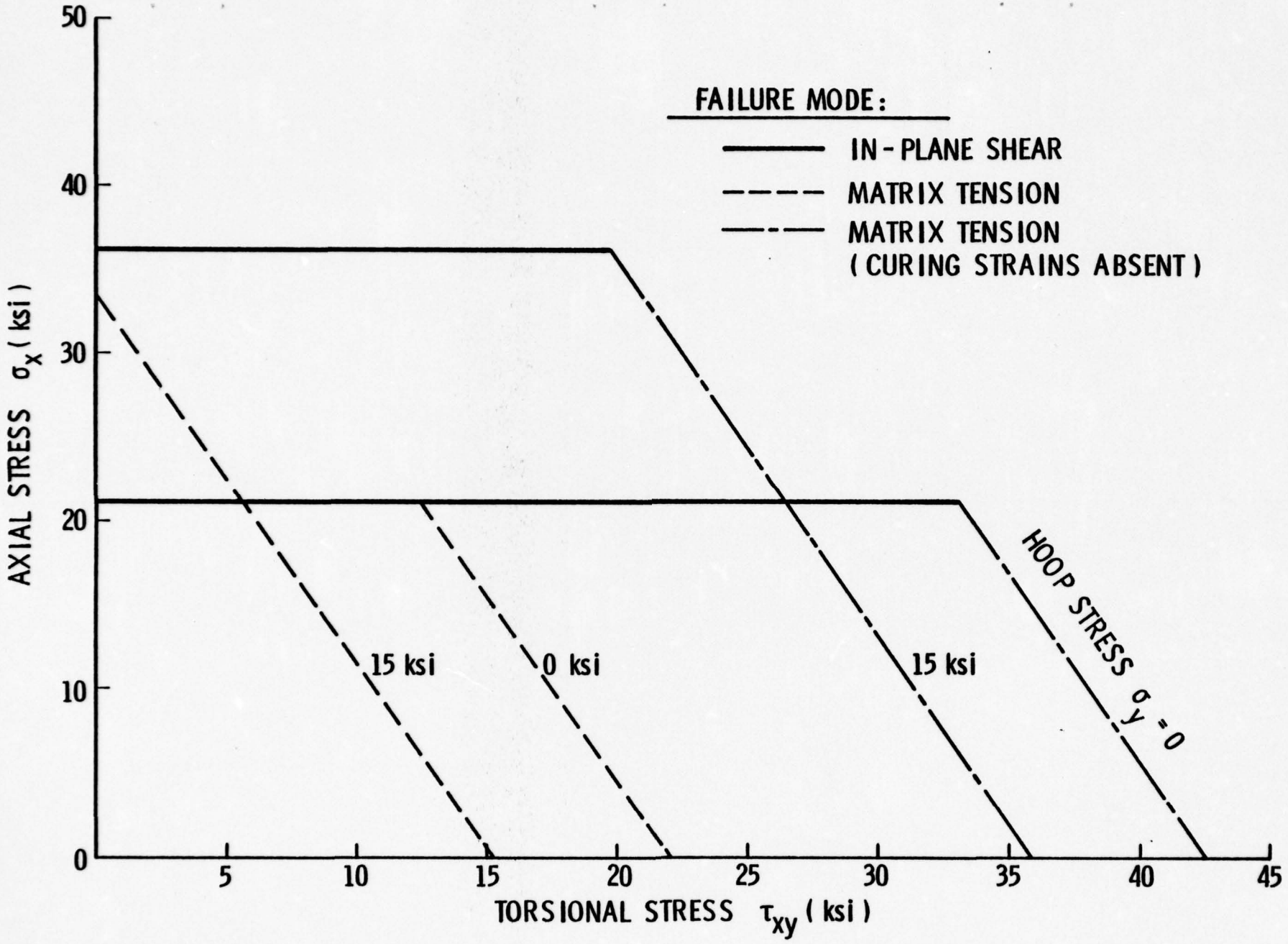

Figure 3. Predicted First Ply Failure Surfaces of $(\pm 45)_s$ Tubes by Laminate Analysis

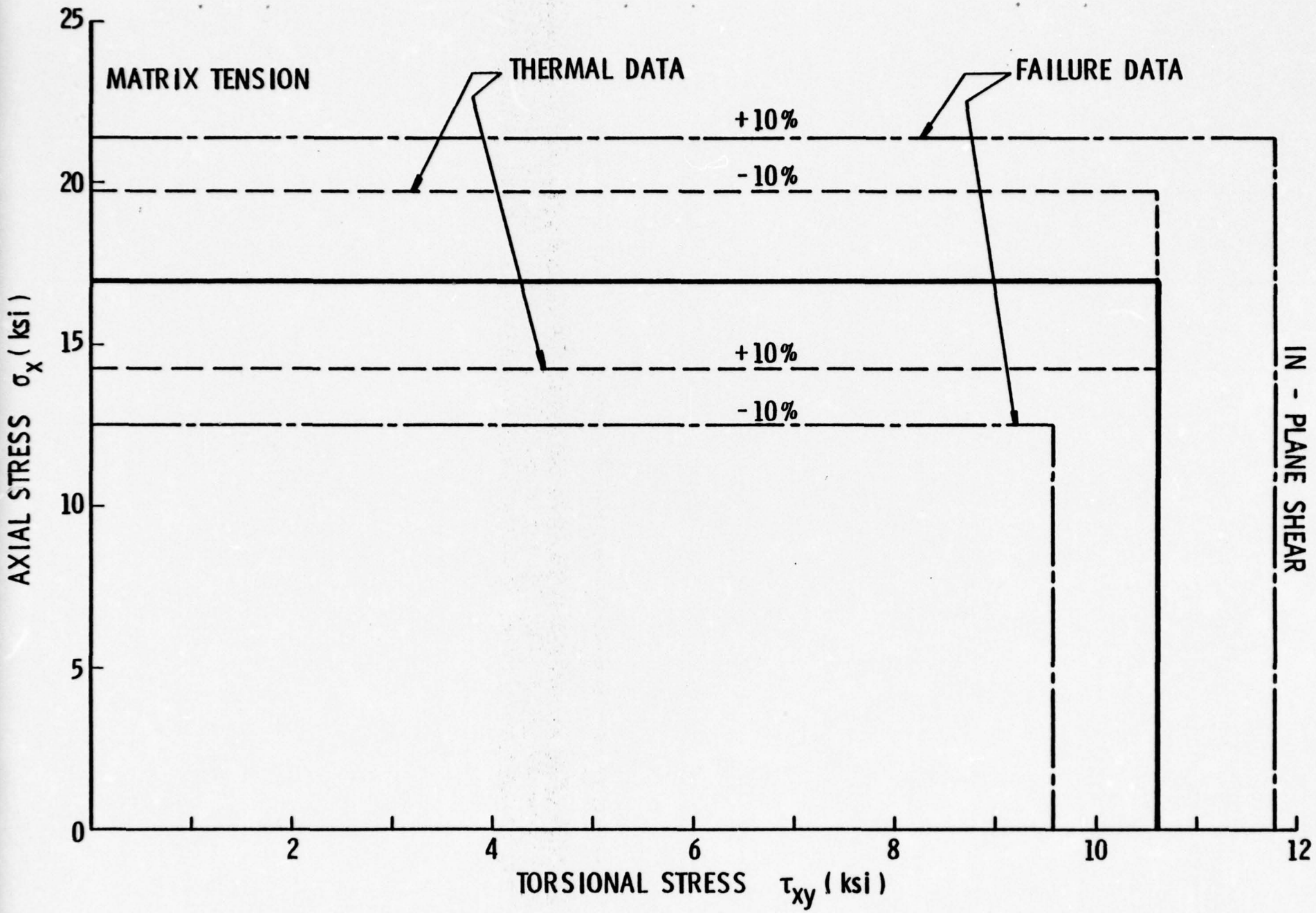

Figure 4. FPF Prediction Input Data Variation $(0/90)_s$

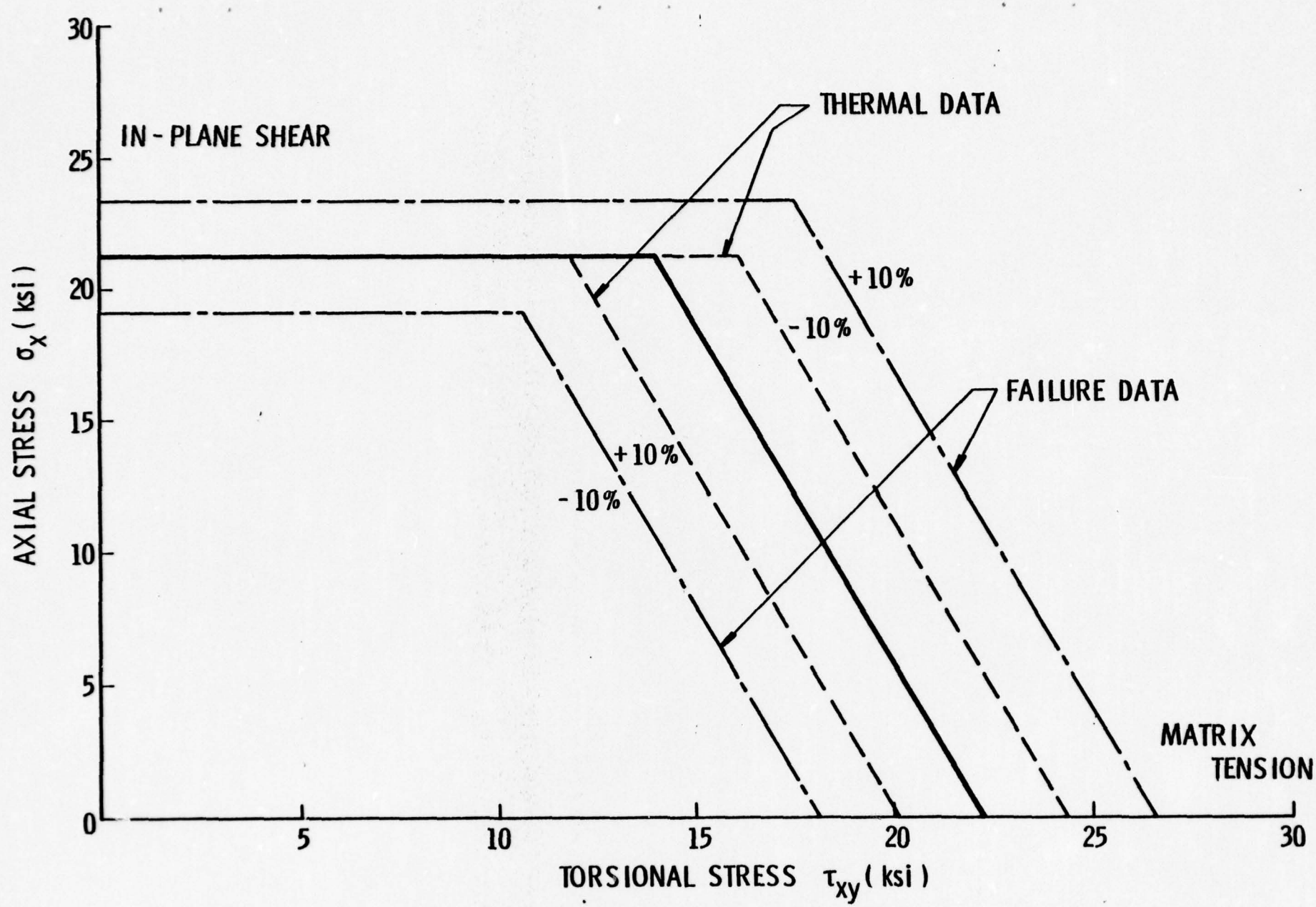

Figure 5. FPF Prediction Input Data Variation $(\pm 45)_s$

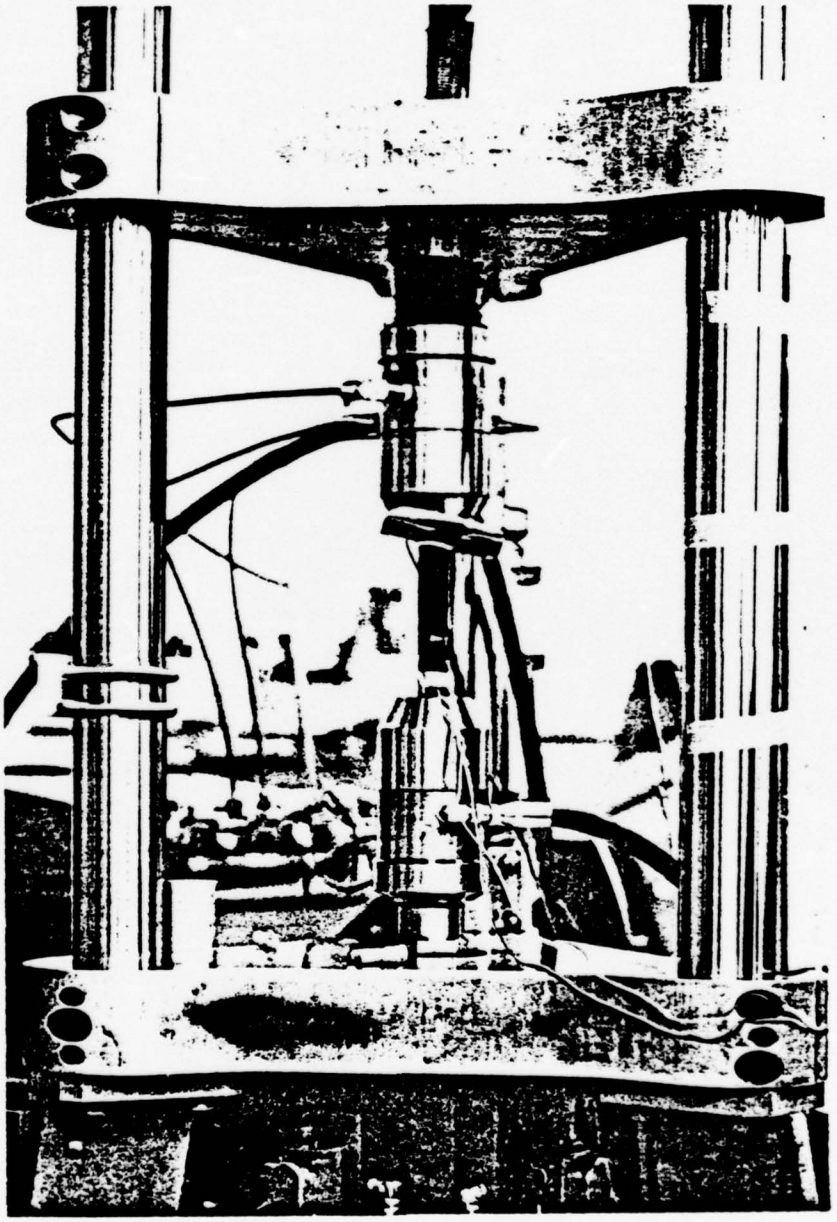

Figure 6. Tubular Specimen Mounted in the Biaxial Machine

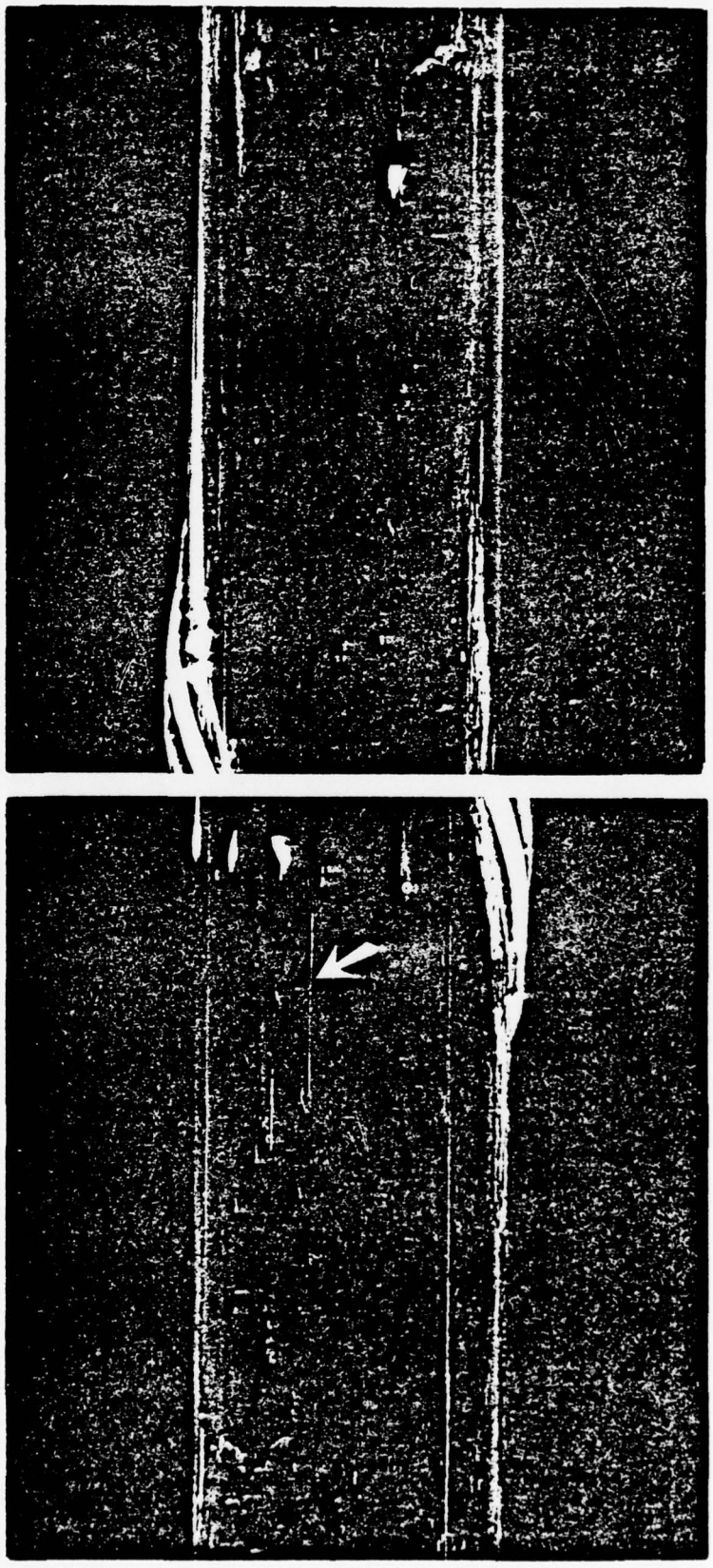

Figure 7. Dye Detected FPF in a $[0/90]_s$ Tube.
FPF Detected with Fluorescent Dye
Penetrant in $[0/90]_s$ Tube.

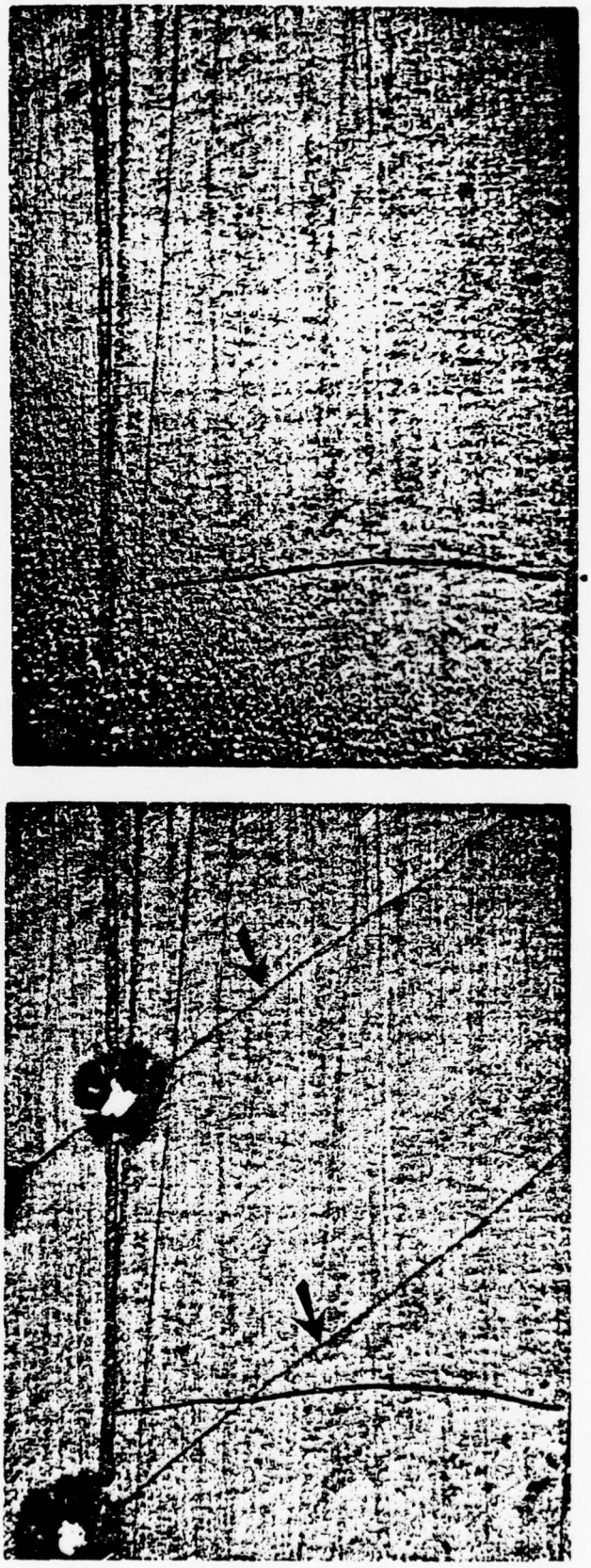

Figure 8. FPF Detected by Replication Techniques in a $[\pm 45]_s$ Tube

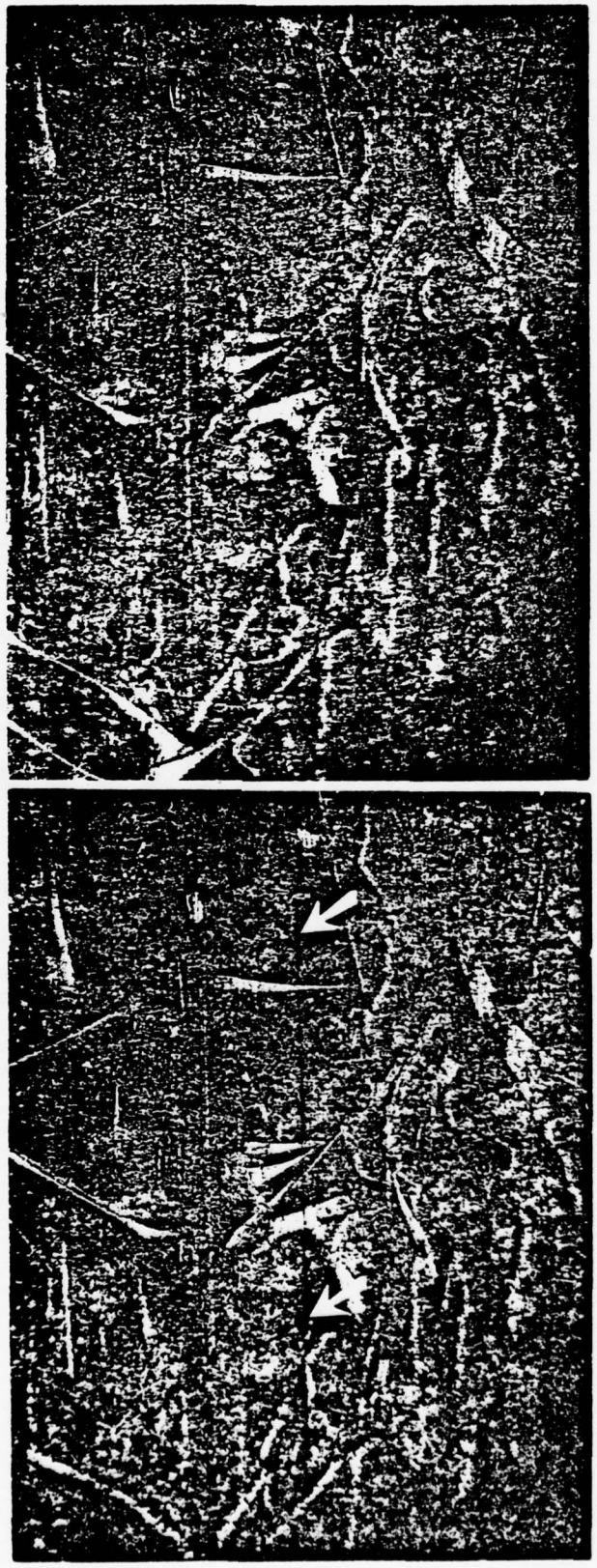

Figure 9. FPF Detected by Replication Techniques in a $[0/90]_s$ Tube

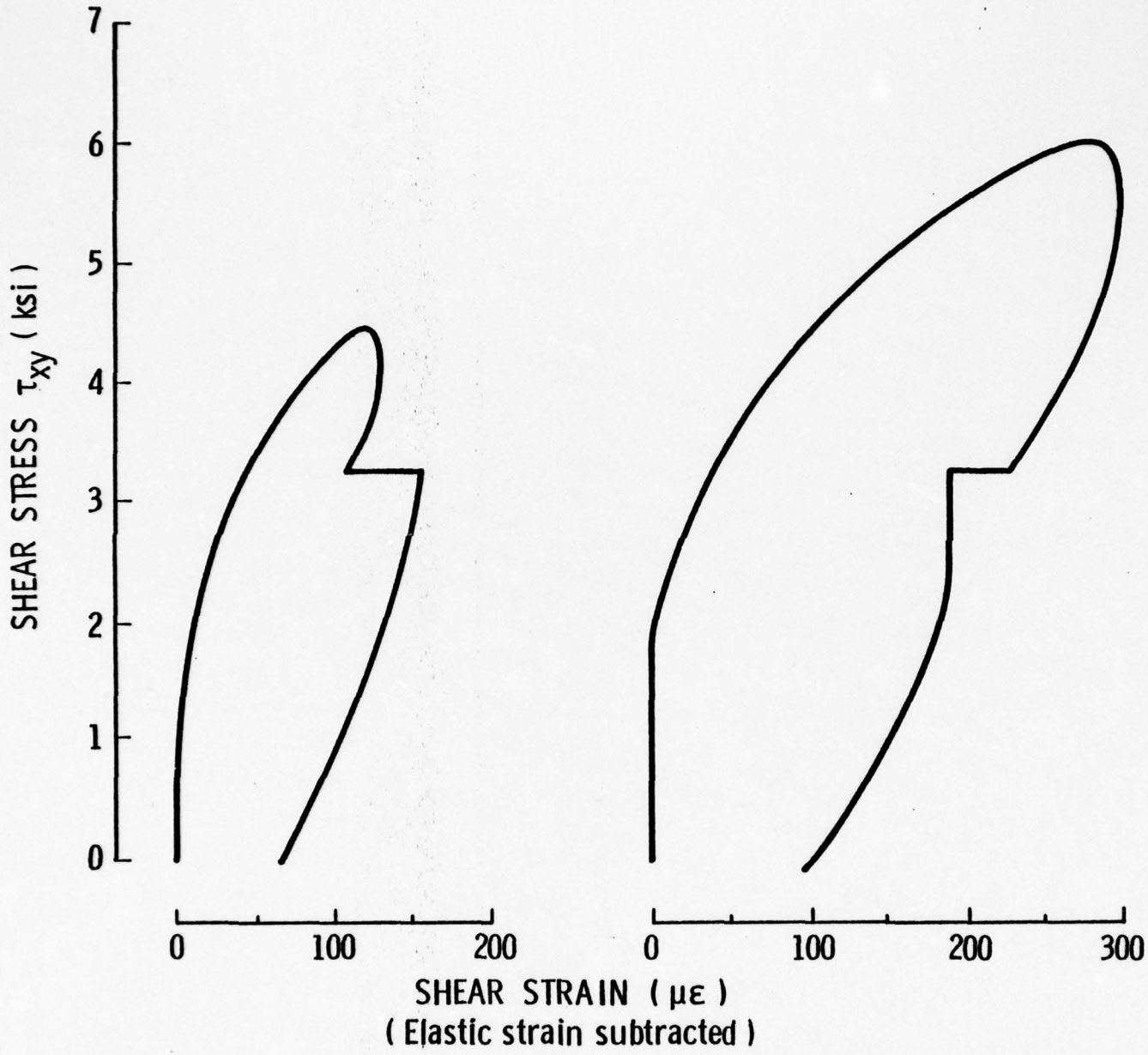

Figure 10. Mechanical Hysteresis in Tube No. 40 $[0/90]_s$, Loaded in Shear

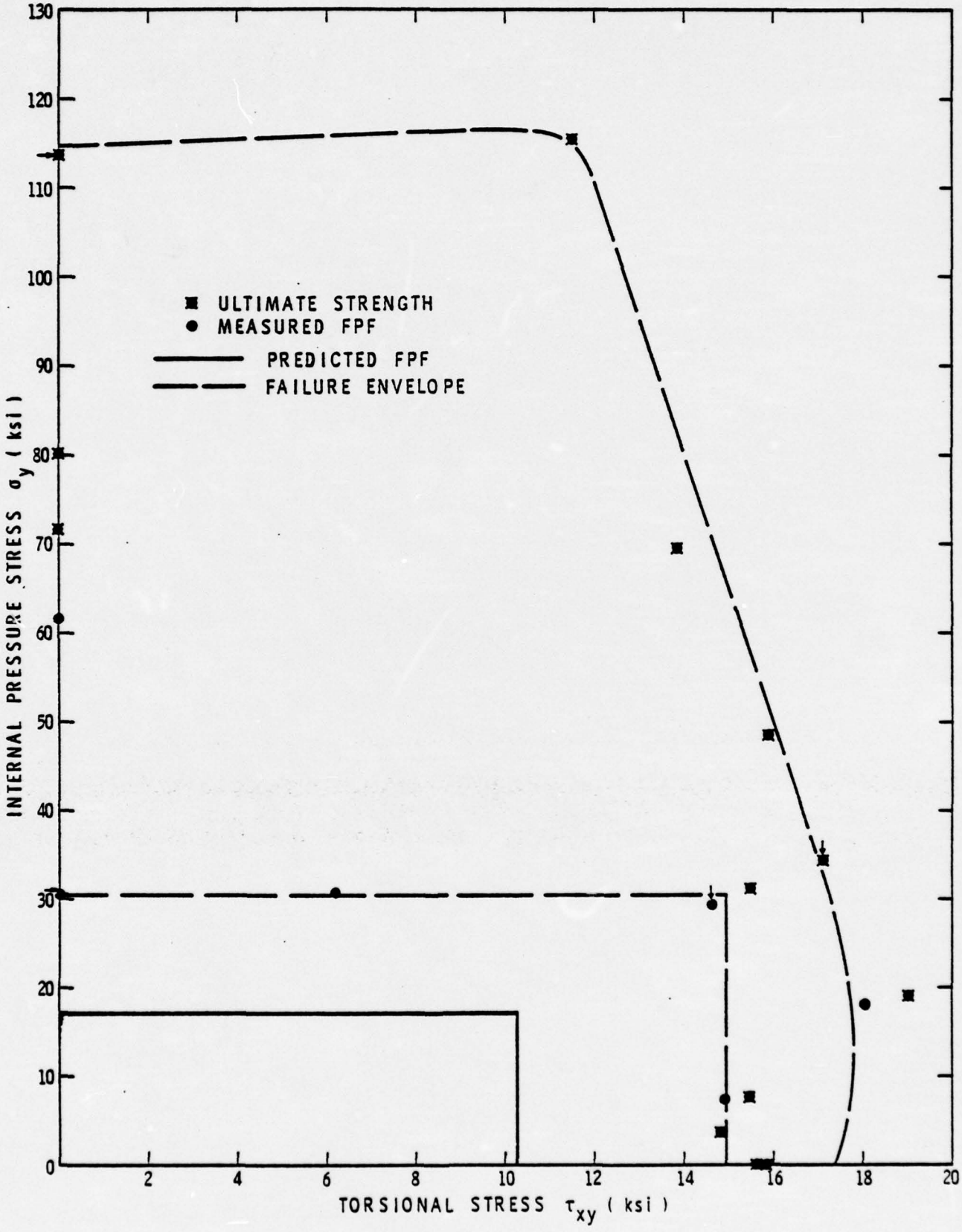

Figure 11. Experimental FPF Measurements on $(0/90)_s$ Tubes

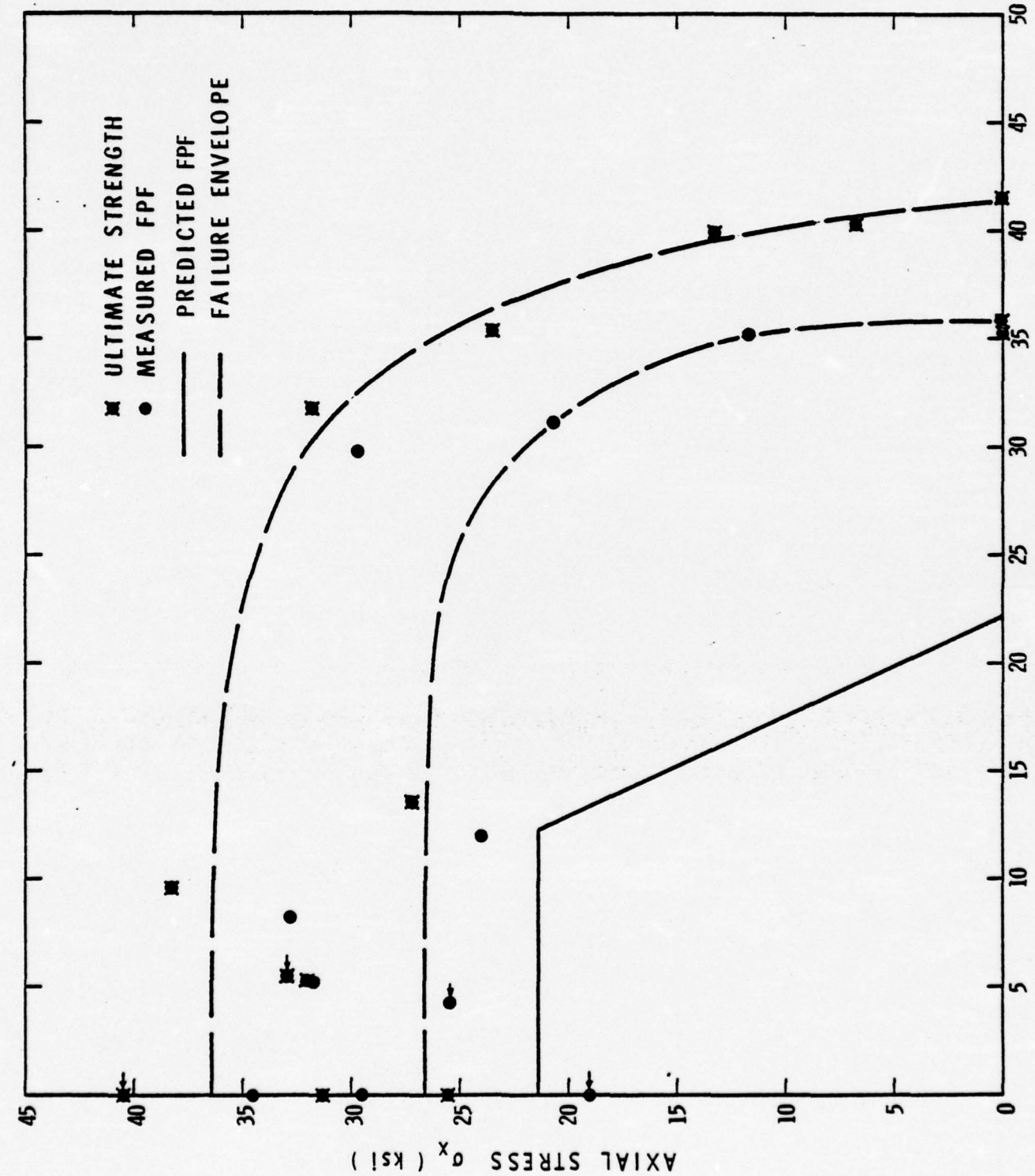

Figure 12. Experimental FPF Measurements on $(\pm 45)_8$ Tubes

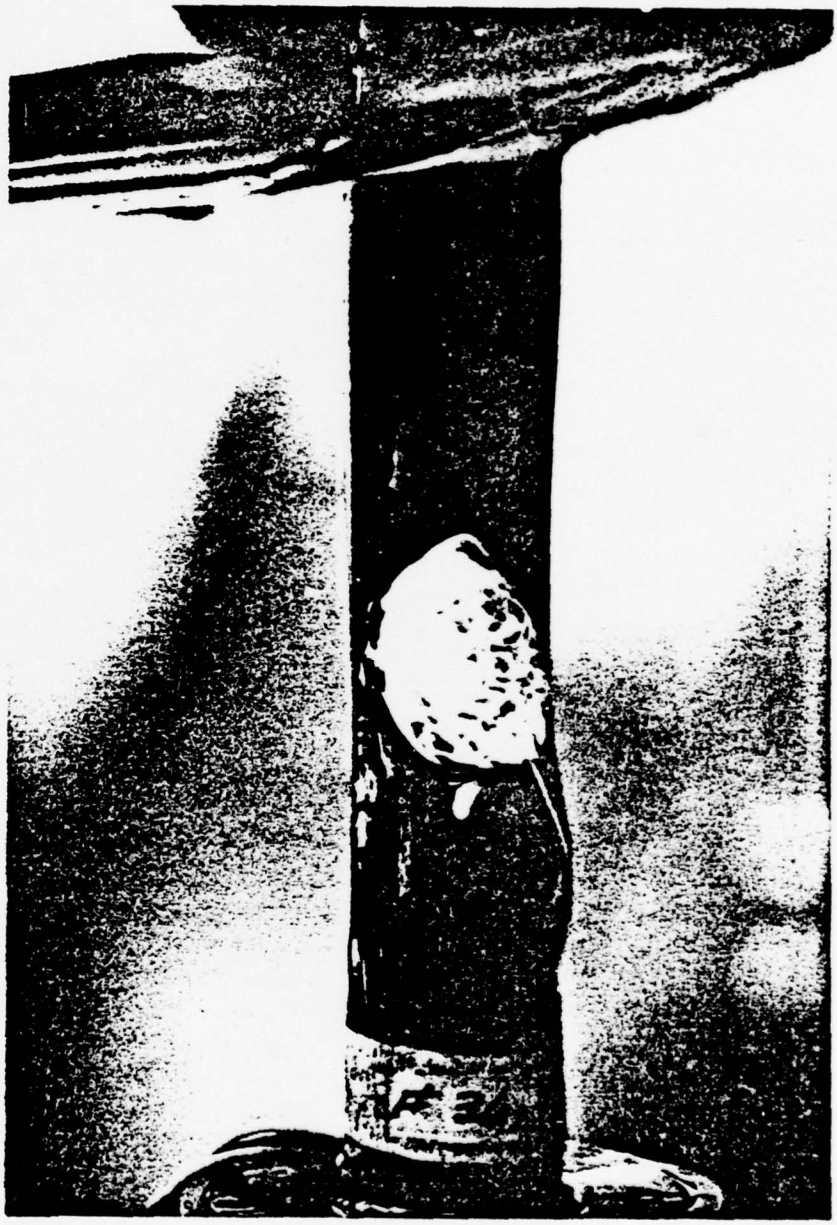

Figure 13. Tube Number 36 After Failing in Torsion

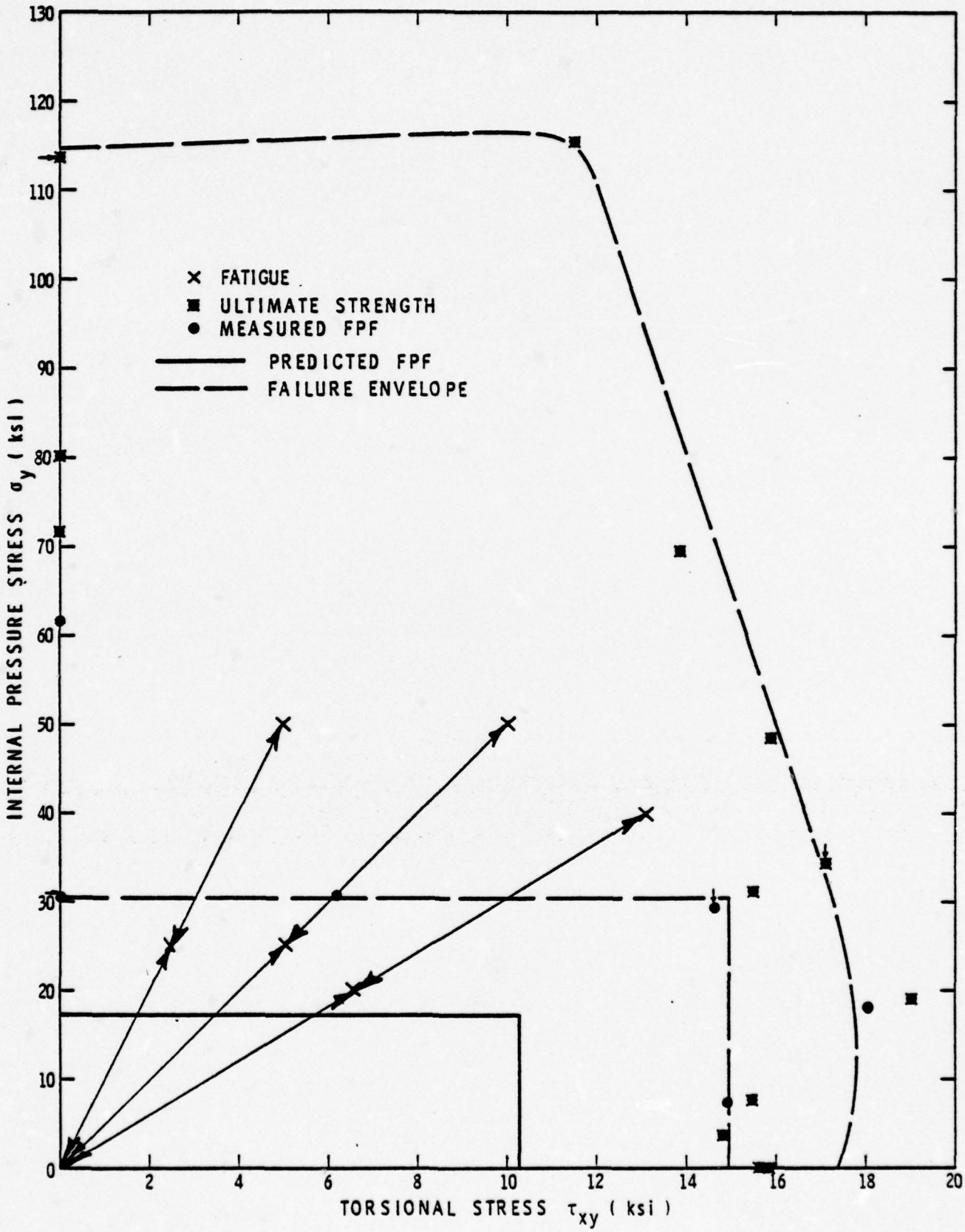

Figure 14. Fatigue Test Peak Stresses for $(0/90)_s$ Tubes.

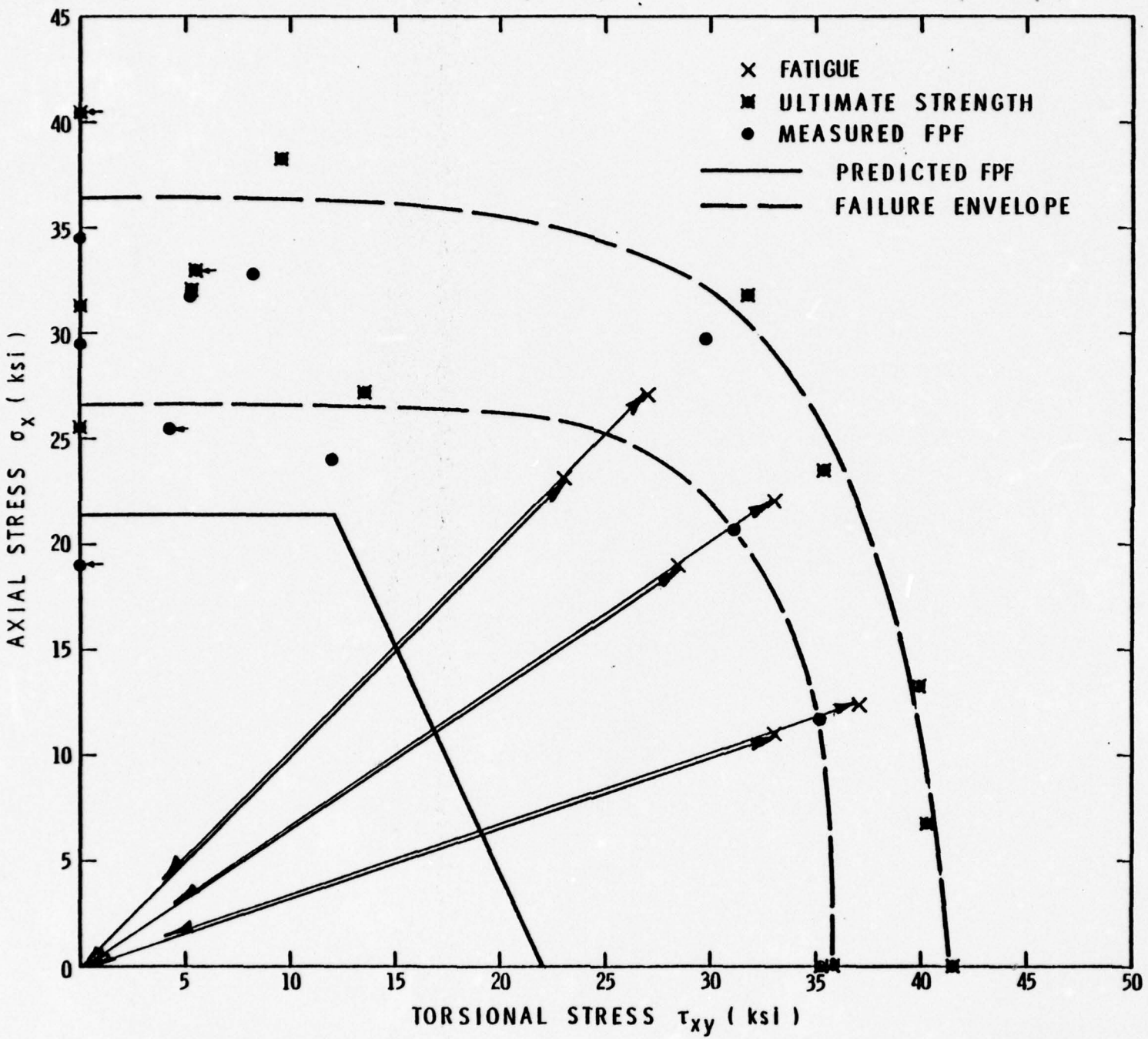

Figure 15. Fatigue Test Peak Stresses for $(\pm 45)_s$ Tubes.

APPENDIX A

FPF CHARACTERIZATION SPECIMENS

$[0/90]_s$ TUBES


124


36


37


43


44

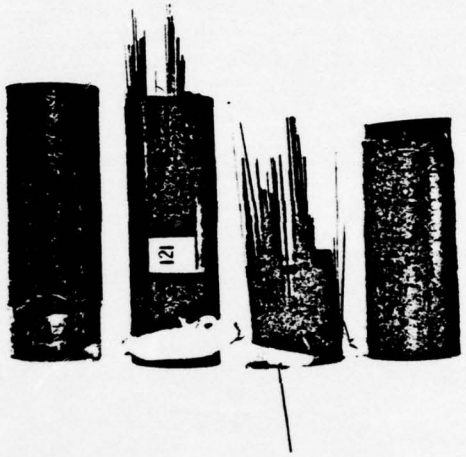
121


45


18

126
41
123
42

$[\pm 45]_s$ TUBES

32
48
119
47

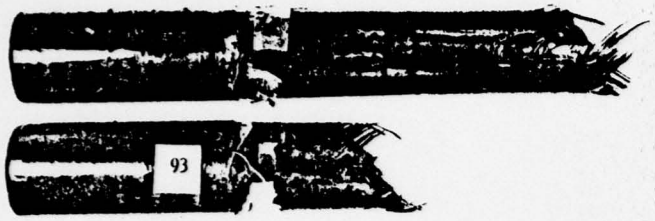
93


88


90


52


96


106


92


89


107


21

APPENDIX B

FATIGUE SPECIMENS

$[0/90]_s$ TUBES

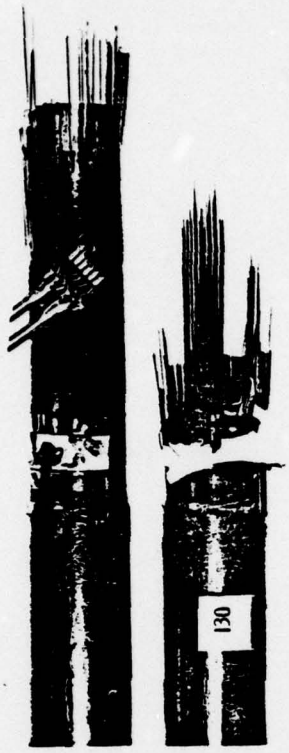
130


121


120


221


125

$[\pm 45]_s$ TUBES


144

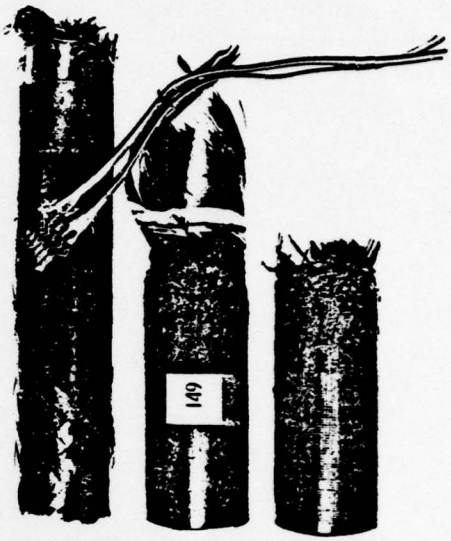
149


147


141


148


154